Journal of Statistics Applications & Probability Letters
An International Journal

http://dx.doi.org/10.18576/jsapl/120102

Modified Alpha Power Transformed Inverse Power Lomax Distribution with applications

Adoté Hervé Gildas Akueson [1,2,4,*], *Mahoulé Jude Bogninou*[3], *Arcadius Yves Justin Akossou* [2] *and Hamidou Bah* [1]

[1]Département d'Agriculture , Institut Supiérieur Agronomique et Vétérinaire Valery Giscard d'Estaing de Faranah (ISAV-VGE/F), BP : 131 Faranah, République de Guinée
[2]Unit of Applied Statistics and Informatics (USIA), Laboratory of Studies and Research in Forestry (LERF) , University of Parakou , Parakou BP 123, Benin
[3]National Higher School of Mathematics Genius and Modelization, National University of Sciences, Technologies, Engineering and Mathematics, Abomey, Benin Republic
[4]Institut de Recherche et de Développement des Plantes Médicinales et Alimentaires, République de Guinée

Received: 2 Oct. 2024, Revised: 23 Feb. 2025, Accepted: 5 Mar. 2025
Published online: 1 Jan. 2025

Abstract: This research introduces the Modified Alpha Power Transformed Inverse Power Lomax Distribution (MAPT-IPLD), a novel and flexible distribution designed to model complex datasets effectively. By integrating the modified alpha power transformation with the inverse power Lomax distribution, the MAPT-IPLD emerges as a robust extension capable of addressing diverse statistical modeling challenges.We present a thorough exploration of the theoretical properties of the MAPT-IPLD, including its stochastic functions, quantile function, moments, probability-weighted moments, and Rényi entropy. Additionally, we derive closed-form expressions for key statistical measures, providing a strong foundation for practical applications.To validate the practical utility of the MAPT-IPLD, we apply it to multiple real-world datasets. The proposed distribution demonstrates superior performance compared to existing models, as evidenced by its ability to achieve the lowest values across a range of information criteria, such as AIC, BIC, HQIC, and K-S statistics. Furthermore, the MAPT-IPLD delivers excellent goodness-of-fit, as visualized through estimated density plots and Q-Q plots, showcasing its ability to accurately capture underlying data structures.These results highlight the MAPT-IPLD's potential as a versatile and reliable tool for statistical modeling across various domains, including reliability analysis, survival studies, and environmental data modeling. By offering a balance between flexibility and parsimony, the MAPT-IPLD sets a new benchmark in the field of statistical distributions.

Keywords: Modified Alpha Power Transformed, Inverse Power Lomax Distribution,statistical modeling, maximum likelihood.

1 Introduction

Statistical distributions are essential tools in quantitative analysis across a wide range of scientific disciplines, providing critical support for predictive modeling and decision-making processes. Their significance spans various domains, including finance, engineering, environmental science, and healthcare. Over time, the landscape of statistical distributions has undergone significant evolution, marked by the introduction of novel families aimed at improving flexibility and adaptability in modeling complex datasets.

In recent years, researchers have witnessed the emergence of diverse distribution families tailored to specific modeling needs. These families, such exponential-G family [1], beta-G family [2], gamma-G family [3], have proven their effectiveness in addressing a broad spectrum of statistical challenges. Furthermore, advancements in statistical distributions have led to the development of innovative families like the Kumaraswamy-G family, half-logistic-G family of type II, and the generalized odd log-logistic Poisson family, each offering customized solutions for modeling datasets with unique characteristics.

Others works include Kumaraswamy Inverted Topp-Leone distribution with applications to COVID-19 Data [4] Poisson-G [5], new power Topp–Leone (TL) generated family of distributions [6], Topp-Leone Cauchy family of

* Corresponding author e-mail: akueson2009@yahoo.fr

© 2025 NSP
Natural Sciences Publishing Cor.

Distributions [7], generalized Odd gamma-G family of distributions [3], Topp–Leone Modified Weibull model [8], Topp–Leone Lomax (TLLo) distribution [9], Marshall-Olkin Topp Leone-G family of distributions [10], arctan power distribution [11], type II generalized Topp-Leone family of distributions [12], new power Topp–Leone generated family of distributions [6], logistic-uniform distribution [13], gamma-uniform distribution [14], uniform distribution of Heegner points [15], Topp-Leone odd log-logistic family of distributions [16], type II exponentiated Half-Logistic-Topp-Leone-G Power Series Class of Distributions [17], Topp Leone power Lomax distribution [18], exponentiated half logistic-Topp-Leone-G power series class of distributions [19], extended generalized exponential power series distribution[20], new inverted Topp-Leone distribution [21], Kumaraswamy inverted Topp–Leone distribution [4], power Lambert uniform distribution [22], step stress and partially accelerated life testing [23], new power Topp–Leone distribution [24], type II power Topp-Leone Daggum distribution [25], new hyperbolic sine-generator [26], type II Topp-Leone Bur XII distribution [27], exponentiated Topp-Leone distribution [28], Kumaraswamy distribution [29] transmuted Kumaraswamy distribution [30], exponentiated Kumaraswamy distribution [31], inverted Kumaraswamy distribution [32], unit-Weibull distribution as an alternative to the Kumaraswamy distribution [33], inflated Kumaraswamy distributions [34], generalized inverted Kumaraswamy distribution [35], bivariate Kumaraswamy distribution [36], Topp-Leone-Marshall-Olkin-G family of distributions [37], type II Topp-Leone generated family of distributions [38], Topp-Leone Gompertz-G family of distributions [39], two-sided generalized Topp-Leone (TS-GTL) distributions [40], Marshall-Olkin extended inverted Kumaraswamy distribution [41], Marshall-Olkin Kumaraswamy distribution [42], Kumaraswamy-geometric distribution [43], Kumaraswamy-log-logistic distribution [44], Kumaraswamy Pareto distribution [45], Topp Leone generalized inverted Kumaraswamy distribution [46].

Despite the progress made, there are still challenges in effectively capturing the complexities of real-world datasets using existing distribution families. Real-life datasets often exhibit complex features such as high skewness, kurtosis, or multimodality, presenting significant obstacles for traditional distribution models. Consequently, there is a growing demand for distribution families that are more flexible and adaptable to the diverse characteristics of modern datasets.

In response to these challenges, our research aims to contribute to the evolving landscape of statistical distributions by introducing a novel distribution tailored to address the complexities of real-life datasets. Drawing on the principles of established distribution families, our approach seeks to develop a new distribution framework capable of accommodating the intricacies of modern datasets. By leveraging innovative methodologies and insights, we aim to create a distribution framework that offers enhanced adaptability and robustness, empowering researchers to effectively model complex datasets and gain deeper insights into diverse phenomena.

In our endeavor to introduce a novel distribution, we have combined the modified version of the Alpha Power Transformation with the Inverse Power Lomax distribution [47]. The Alpha Power Transformation (APT) [48] has garnered considerable attention in recent years for its capacity to introduce innovative distributions, thereby enhancing flexibility in statistical modeling. This technique, referred to as the alpha power transformation (APT), has been pivotal in integrating skewness into distribution models, resulting in the development of several generalized distributions. The cumulative distribution function (CDF) and probability density function (PDF) of the APT method are expressed as follows:

$$F_{\text{APT}}(x) = \begin{cases} \frac{\alpha^{G(x)}-1}{(\alpha-1)}, & \alpha > 0, \text{ and } \alpha \neq 1 \\ G(x), & \alpha = 1 \end{cases}$$

$$f_{\text{APT}}(x) = \begin{cases} \frac{\log(\alpha)}{(\alpha-1)} g(x)\alpha^{G(x)}, & \alpha > 0, \text{ and } \alpha \neq 1 \\ g(x), & \alpha = 1 \end{cases}$$

Notable examples include the alpha power Weibull distribution [49], alpha power transformed extended exponential distribution [50], alpha power transformed inverse Lindley distribution [51],alpha power Gompertz distribution [52], alpha power transformed Inverse Lomax [53], Alpha-Power Transformed Lomax Distribution [54],

To further enhance the versatility of the APT method, Alotaibi et al. [55] proposed a modified version known as the Modified Alpha Power Transformation (MAPT) method. This refined method introduces an additional term, enabling greater customization and refinement in modeling diverse datasets. Expanding upon the MAPT framework, researchers have devised a range of distributions, including the Modified Alpha Power Transformed Weibull Distribution [56].

Similarly, the cumulative distribution function (CDF) and probability density function (PDF) of the MAPT method are given by:

$$F_{\text{MAPT}}(x) = \begin{cases} \frac{\alpha^{G(x)}-1}{(\alpha-1)\left(1+\alpha-\alpha^{G(x)}\right)}, & \alpha > 0 \text{ and } \alpha \neq 1 \\ G(x), & \alpha = 1 \end{cases}$$

© 2025 NSP
Natural Sciences Publishing Cor.

$$f_{\text{MAPT}}(x) = \begin{cases} \frac{\alpha^{1+G(x)}\log(\alpha)g(x)}{(\alpha-1)\left(1+\alpha-\alpha^{G(x)}\right)^2}, & \alpha > 0 \text{ and } \alpha \neq 1 \\ g(x), & \alpha = 1 \end{cases}$$

Our primary objective in this article is to introduce a novel version of the Inverse Power Lomax distribution utilizing the MAPT method. By leveraging the MAPT approach, we aim to introduce a new shape parameter into the baseline Cumulative Distribution Function (CDF), thereby enhancing the distribution's adaptability and versatility in modeling diverse datasets.

Introducing the Inverse Power Lomax distribution [47], a versatile distribution renowned for its application in modeling various phenomena. The cumulative distribution function (CDF) and the probability density function (PDF) of the Inverse Power Lomax distribution are as follows:

$$G(x;\lambda,b,\beta) = \left(1+\frac{x^{-\beta}}{b}\right)^{-\lambda} \tag{1}$$

$$g(x;\lambda,b,\beta) = \frac{\lambda\beta}{b}x^{-\beta-1}\left(1+\frac{x^{-\beta}}{b}\right)^{-\lambda-1} \tag{2}$$

These formulas define the behavior of the distribution, where x represents the random variable, λ is the shape parameter, b is the scale parameter, and β is an additional shape parameter. The Inverse Power Lomax distribution offers a flexible framework for modeling various datasets, with its parameters allowing for customization to suit different scenarios.

2 Modified Alpha Power Transformation - Inverse Power Lomax Distribution (MAPT-IPL)

The MAPT-IPLD (Modified Alpha Power Transformation - Inverse Power Lomax Distribution) emerges as a novel fusion, combining the enhanced flexibility of the MAPT method with the versatile modeling capabilities of the Inverse Power Lomax distribution. The cumulative distribution function (CDF) and the probability density function (PDF) of the MAPT-IPLD distribution with $x \in]0;+\infty[$ are given by:

$$F_{\text{MAPT-IPL}}(x) = \begin{cases} \frac{\alpha^{\left(1+\frac{x^{-\beta}}{b}\right)^{-\lambda}}-1}{(\alpha-1)\left(1+\alpha-\alpha^{\left(1+\frac{x^{-\beta}}{b}\right)^{-\lambda}}\right)}, & \alpha > 0 \text{ and } \alpha \neq 1 \\ \left(1+\frac{x^{-\beta}}{b}\right)^{-\lambda}, & \alpha = 1 \end{cases} \tag{3}$$

$$f_{\text{MAPT-IPL}}(x) = \begin{cases} \frac{\lambda\beta}{b}\frac{\log(\alpha)}{(a-1)}x^{-\beta-1}\left(1+\frac{x^{-\beta}}{b}\right)^{-\lambda-1}\frac{\alpha^{1+\left(1+\frac{x^{-\beta}}{b}\right)^{-\lambda}}}{\left(1+\alpha-\alpha^{\left(1+\frac{x^{-\beta}}{b}\right)^{-\lambda}}\right)^2} & \alpha > 0 \text{ and } \alpha \neq 1 \\ \frac{\lambda\beta}{b}x^{-\beta-1}\left(1+\frac{x^{-\beta}}{b}\right)^{-\lambda-1}, & \alpha = 1 \end{cases} \tag{4}$$

These formulas elucidate the behavior of the MAPT-IPLD distribution, where x represents the random variable, λ is the shape parameter, b is the scale parameter, and β is an additional shape parameter.

The integration of the MAPT method with the Inverse Power Lomax distribution offers several compelling advantages. Firstly, it enhances the distribution's adaptability to capture the intricacies of real-world datasets characterized by complex features such as skewness, kurtosis, and multimodality. Additionally, the MAPT-IPLD distribution provides researchers with a robust framework for modeling diverse phenomena across various domains, from finance and engineering to environmental science and healthcare.

Furthermore, the MAPT-IPLD distribution offers ease of interpretation and implementation, making it a valuable tool for both practitioners and researchers in statistical modeling and analysis. Its ability to accommodate a wide range of scenarios and datasets underscores its relevance and utility in contemporary statistical practice.

© 2025 NSP
Natural Sciences Publishing Cor.

Figure 1 and figure 2 provide valuable insights into the behavior and characteristics of the distribution, offering a deeper understanding of its modeling capabilities.

In the CDF plot (Figure 1), we observe the cumulative probability distribution of the MAPT-IPLD distribution across a range of values for the random variable x. The plot illustrates how the distribution accumulates probability as x increases, visually representing the distribution's shape and spread. Possible comments on the CDF plot may include discussions on the distribution's skewness, tail behavior, and overall variability.

Transitioning to the PDF plot (Figure 2), we examine the probability density function of the MAPT-IPLD distribution, illustrating the likelihood of observing different values of x within a given interval. This plot provides insights into the distribution's probability density at various points along the range of x, revealing its peaks, troughs, and areas of high concentration. Comments on the PDF plot may focus on the distribution's mode(s), spread, and symmetry or asymmetry.

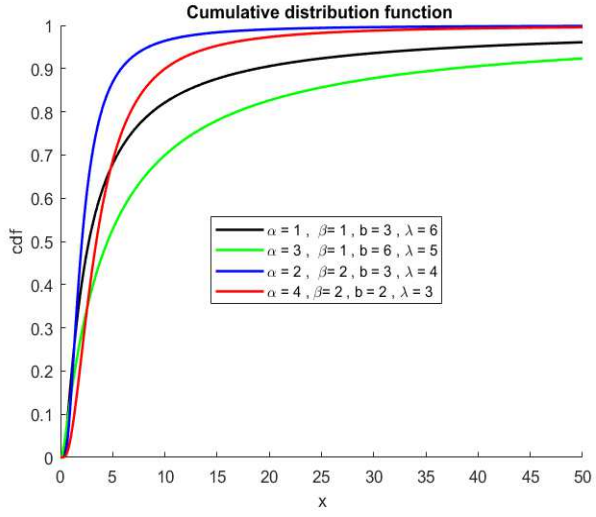

Various sets of parameters

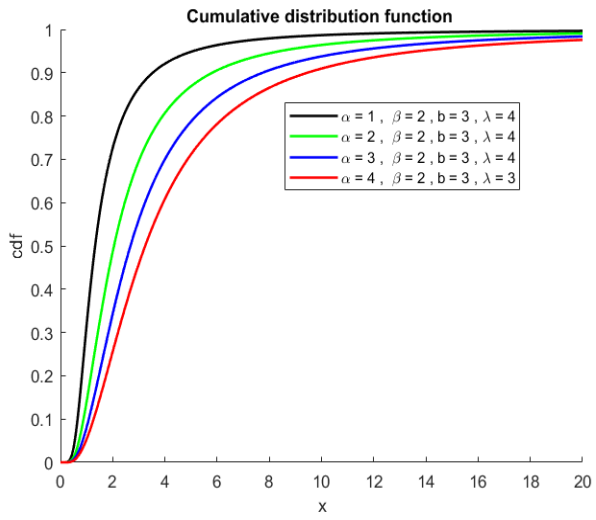

Various values of fixed

Fig. 1: MAPT-IPLD's Cumulative distribution functions

Now, let's explore the reliability function (RF) and the hazard rate function (HRF) for the MAPT-IPLD (Modified Alpha Power Transformation - Inverse Power Lomax Distribution). These functions provide crucial insights into the

© 2025 NSP
Natural Sciences Publishing Cor.

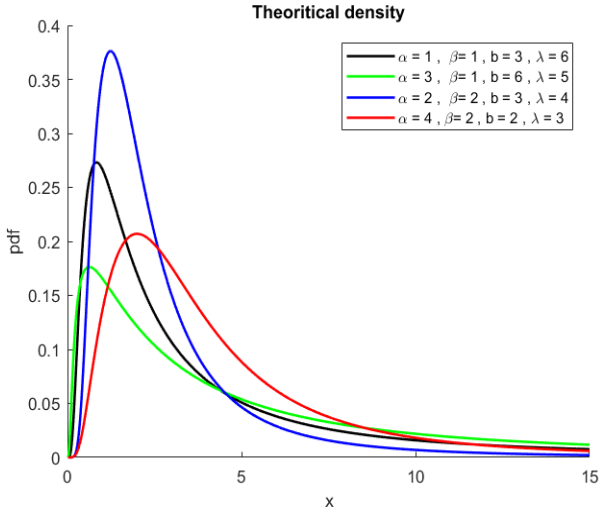

Various sets of parameters

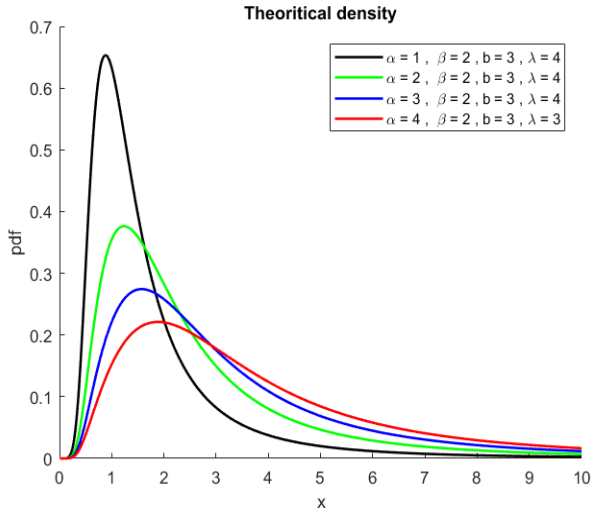

Various values of fixed

Fig. 2: MAPT-IPLD's robability density function

survival characteristics and failure rates associated with the distribution, offering valuable information for reliability analysis and risk assessment. The reliability or survival function $R_{\text{MAPT}}(x)$ of the MAPT-IPLD is given by:

$$R_{\text{MAP-IPLT}}(x) = \begin{cases} 1 - \dfrac{\alpha^{\left(1+\frac{x^{-\beta}}{b}\right)^{-\lambda}} - 1}{(\alpha-1)\left(1+\alpha-\alpha^{\left(1+\frac{x^{-\beta}}{b}\right)^{-\lambda}}\right)}, & \alpha > 0 \text{ and } \alpha \neq 1 \\ 1 - \left(1+\frac{x^{-\beta}}{b}\right)^{-\lambda}, & \alpha = 1 \end{cases}$$

This function represents the probability that the MAPT-IPLD variable x exceeds a given value, providing insights into its survival characteristics over time.

© 2025 NSP
Natural Sciences Publishing Cor.

Moving on, the hazard rate function $h_{\text{MAPT}}(x)$ of the MAPT-IPLD is calculated as the ratio of the probability density function $f_{\text{MAPT}}(x)$ to the complement of the reliability function $R_{\text{MAPT}}(x)$, expressed as:

$$h_{\text{MAPT}}(x) = \frac{f_{\text{MAPT-IPLD}}(x)}{R_{\text{MAPT}}(x)} \tag{5}$$

This function quantifies the instantaneous failure rate at time x, providing insights into the likelihood of failure at different points in time.

To further illustrate the behavior of the reliability and hazard rate functions for the MAPT-IPLD distribution, we present corresponding plots that offer visual insights into the distribution's survival characteristics and failure rates.

The figure 3 depicting the reliability function $R_{\text{MAPT}}(x)$ showcases how the probability of survival evolves over time, providing a clear visualization of the distribution's ability to withstand failures.

Moving on to the hazard rate function $h_{\text{MAPT}}(x)$, the accompanying figure 4 illustrates the instantaneous failure rate at different time points x. This plot offers valuable insights into the likelihood of failure occurrence at various stages, helping to identify critical time intervals and assess reliability performance.

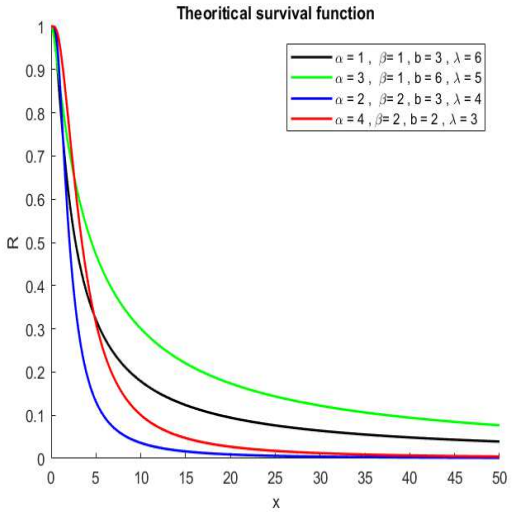

Fig. 3: MAPT-IPLD's survival function

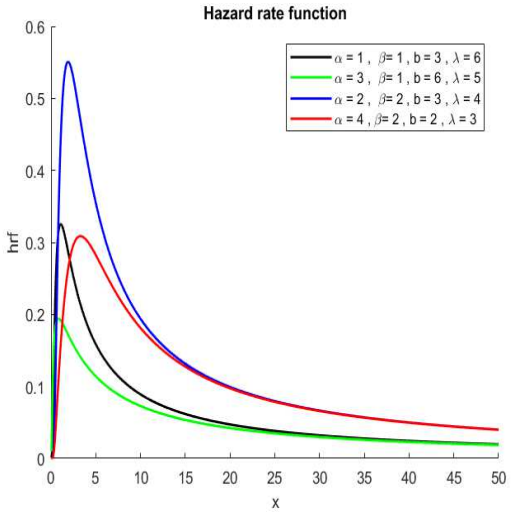

Fig. 4: MAPT-IPLD's hazard rate function

3 Mixture Representation of the MAPT-IPL Distribution

To unveil the core properties of the MAPT-IPL distribution, we present an insightful expansion for its probability density function (PDF). The PDF takes the following form:

$$f(x) = \frac{\lambda\beta}{b}\frac{\alpha\log(\alpha)}{(a-1)(\alpha+1)^2}x^{-\beta-1}\left(1+\frac{x^{-\beta}}{b}\right)^{-\lambda-1}\alpha^{\left(1+\frac{x^{-\beta}}{b}\right)^{-\lambda}}\left(1-\frac{\alpha^{\left(1+\frac{x^{-\beta}}{b}\right)^{-\lambda}}}{\alpha+1}\right)^{-2} \quad \text{for } \alpha>0 \text{ and } \alpha\neq 1 \tag{6}$$

We commence by considering the following power series:

$$\alpha^y = \sum_{m=0}^{\infty}\frac{(\log\alpha)^m}{m!}y^m. \tag{7}$$

© 2025 NSP
Natural Sciences Publishing Cor.

and the generalized binomial expansion:

$$(1-y)^{-2} = \sum_{k=0}^{\infty} (k+1)y^k, \quad |y| < 1. \tag{8}$$

By employing the series in (7) and (8), we express the PDF in (6) as a mixture representation of inverse power Lomax densities:

$$f(x) = \sum_{m=0}^{\infty} T_{m,k} g(x; (m+1)\lambda, b, \beta) \tag{9}$$

where $g(x; (m+1)\lambda, b, \beta)$ denotes the PDF of the Inverse Power Lomax distribution with scale parameter $(m+1)\lambda$, shape parameter b and additional parameter β. Here,

$$T_{m,k} = \sum_{k=0}^{\infty} \frac{\alpha(k+1)^{m+1}(\log\alpha)^{m+1}}{(\alpha-1)(\alpha+1)^{k+2}(m+1)!}.$$

The structural properties of the MAPT-IPL distribution can be directly inferred from (9) based on the well-known properties of the Inverse Power Lomax distribution. Integrating (9), we can express the expansion of the cumulative distribution function (CDF) of the MAPT-IPL distribution as:

$$F(x) = \sum_{m=0}^{\infty} T_{m,k} G(x; (m+1)\lambda, b, \beta) \tag{10}$$

where $G(x; (m+1)\lambda, b, \beta)$ represents the CDF of the Inverse Power Lomax distribution.

4 Essential Properties of the MAPT-IPL distribution

This section delves into the core statistical properties of the MAPT-IPL distribution, encompassing quantiles, moments, moment generating functions, and order statistics.

4.1 Quantiles and Random Number Generation

Quantiles are indispensable in estimation and simulation endeavors. For the MAPT-IPL distribution, the p-th quantile x_p is defined by the equation:

$$x_p = \frac{1}{b^{\frac{1}{\beta}}} \left\{ \left[\frac{\log(\alpha)}{\log\left(\frac{1+p(\alpha^2-1)}{1+p(\alpha-1)}\right)} \right]^{\frac{1}{\lambda}} - 1 \right\}^{-\frac{1}{\beta}}, \quad 0 < p < 1. \tag{11}$$

In particular, the first three quantiles, $Q1$, $Q2$, and $Q3$, correspond to $p = 0.25$, $p = 0.5$, and $p = 0.75$ in (11) respectively.

To generate a random sample comprising n observations from the MAPT-IPL distribution, one can employ Eq. (11) alongside a uniform random variable $U \sim \text{Uniform}(0,1)$ as follows:

$$x_i = \frac{1}{b^{\frac{1}{\beta}}} \left\{ \left[\frac{\log\alpha}{\log\left(\frac{1+u_i(\alpha^2-1)}{1+u_i(\alpha-1)}\right)} \right]^{\frac{1}{\lambda}} - 1 \right\}^{-\frac{1}{\beta}}, \quad i = 1, \ldots, n. \tag{12}$$

The impact of parameters α and λ on skewness and kurtosis can be assessed through quantile-based measures. Bowley's skewness [57], for instance, is formulated as:

$$B = \frac{Q(3/4) + Q(1/4) - 2Q(1/2)}{Q(3/4) - Q(1/4)}, \tag{13}$$

© 2025 NSP
Natural Sciences Publishing Cor.

where $Q(p)$ represents the p-th quantile. Known for its robustness, Bowley's skewness focuses exclusively on the middle two quartiles, mitigating the influence of outliers. Moors kurtosis [58], another metric, is articulated as:

$$M = \frac{Q(3/8) - Q(1/8) + Q(7/8) - Q(5/8)}{Q(6/8) - Q(2/8)}. \tag{14}$$

Evidently, $M > 0$, aligning well with classical kurtosis measures for specific distributions. Remarkably, these metrics retain significance even for distributions lacking moments, demonstrating resilience against outliers. Figure 6 depicts the 3D plot of kurtosis and skewness utilizing formula (13) and (14).

4.2 Moments and Inverse Moments

Moments are crucial in statistical theory, offering insights into various essential characteristics of distributions. For the MAPT-IPL distribution, the nth moment is given by:

$$\begin{aligned}
\mu_n &= \int_0^\infty x^n f(x)dx = E(X^n) \\
&= \sum_{m=0}^{\infty} T_{m,k} x^n g(x;(m+1)\lambda)dx \\
&= \sum_{m=0}^{\infty} T_{m,k} \int_0^\infty x^n \frac{\lambda(m+1)\beta}{b} x^{-\beta-1} \left(1+\frac{x^{-\beta}}{b}\right)^{-\lambda(m+1)-1} dx \\
&= \sum_{m=0}^{\infty} T_{m,k} \int_0^\infty \frac{\lambda(m+1)\beta}{b} x^{n-\beta-1} \left(1+\frac{x^{-\beta}}{b}\right)^{-\lambda(m+1)-1} dx \\
&\quad n = 1,2,3,\ldots,
\end{aligned} \tag{15}$$

Applying the transformation

$$y = \left(1+\frac{x^{-\beta}}{b}\right)^{-1}, \tag{16}$$

we obtain $dy = \frac{1}{b}\beta x^{-\beta-1}\left(1+\frac{x^{-\beta}}{b}\right)^{-2} dx$, and $0 < y < 1$.
By substituting (16) into equation (15), we have:

$$\mu_n = \sum_{m=0}^{\infty} T_{m,k} \int_0^1 \lambda(m+1) b^{-\frac{n}{\beta}} (1-y)^{-\frac{n}{\beta}} y^{\lambda(m+1)+\frac{n}{\beta}-1} dy$$

Employing the beta function integration, we obtain:

$$\mu_n = \sum_{m=0}^{\infty} T_{m,k} \lambda b^{-\frac{n}{\beta}} B\left(1-\frac{n}{\beta}; \lambda(m+1)+\frac{n}{\beta}\right)$$

where $B(.,.)$ denotes the beta function. Therefore, the nth moment of the MAPT-IPL distribution is given by:

$$\mu_n = \sum_{m=0}^{\infty} T_{m,k} \frac{\lambda b^{-\frac{n}{\beta}} \Gamma\left(1-\frac{n}{\beta}\right) \Gamma\left(\lambda(m+1)+\frac{n}{\beta}\right)}{\Gamma\left(\lambda(m+1)+1\right)} \tag{17}$$

where $\Gamma(.)$ is the gamma function.

Similarly, for the MAPT-IPL distribution, the nth inverse moment can be obtained as follows:

$$E\left(\frac{1}{X^n}\right) = \sum_{m=0}^{\infty} T_{m,k} \frac{\lambda b^{-\frac{n}{\beta}} \Gamma\left(1+\frac{n}{\beta}\right) \Gamma\left(\lambda(m+1)-\frac{n}{\beta}\right)}{\Gamma\left(\lambda(m+1)+1\right)} \tag{18}$$

© 2025 NSP
Natural Sciences Publishing Cor.

Furthermore, the first and second moments of the distribution are expressed as follows:

$$\mu_1 = E(x) = \sum_{m=0}^{\infty} T_{m,k} \frac{\lambda b^{-\frac{1}{\beta}} \Gamma\left(1-\frac{1}{\beta}\right) \Gamma\left(\lambda(m+1)+\frac{1}{\beta}\right)}{\Gamma(\lambda(m+1)+1)} \tag{19}$$

$$\mu_2 = E(x^2) = \sum_{m=0}^{\infty} T_{m,k} \frac{\lambda b^{-\frac{2}{\beta}} \Gamma\left(1-\frac{2}{\beta}\right) \Gamma\left(\lambda(m+1)+\frac{2}{\beta}\right)}{\Gamma(\lambda(m+1)+1)} \tag{20}$$

Similarly, the rth central moment of a given random variable X is defined as:

$$C_r = E(X-\mu_1)^r = \sum_{i=0}^{r} (-1)^i \binom{r}{i} (\mu_1)^i \mu_{r-i} \tag{21}$$

The variance of the MAPT-IPL distribution is obtained as:

$$\begin{aligned} \sigma^2 &= \mu_2 - (\mu_1)^2 \\ &= \sum_{m=0}^{\infty} T_{m,k} \frac{\lambda b^{-\frac{2}{\beta}} \Gamma\left(1-\frac{2}{\beta}\right) \Gamma\left(\lambda(m+1)+\frac{2}{\beta}\right)}{\Gamma(\lambda(m+1)+1)} - (\mu_1)^2. \end{aligned}$$

Figure 5 illustrates the 3D plot of the mean and the variance.

4.3 Moment Generating Function

The moment generating function (MGF) $M_X(t)$ of a random variable X is given by

$$M_X(t) = \sum_{r=0}^{\infty} \sum_{m=0}^{\infty} \frac{(t)^r}{r!} T_{m,k} \frac{\lambda b^{-\frac{r}{\beta}} \Gamma(1-\frac{r}{\beta}) \Gamma(\lambda(m+1)+\frac{r}{\beta})}{\Gamma(\lambda(m+1)+1)}. \tag{22}$$

Proof. The Moment Generating Function of the positive random variable X with probability density function $f(x)$ is given by

$$M_X(t) = \int_0^{\infty} e^{tx} f(x) dx \tag{23}$$

Using series expansion of e^{tX},

$$M_X(t) = \sum_{r=0}^{\infty} \frac{(t)^r}{r!} \int_0^{\infty} x^r f(x) dx = \sum_{r=0}^{\infty} \frac{(t)^r}{r!} E(X^r), \tag{24}$$

Substituting from (17) into (24),

$$M_X(t) = \sum_{r=0}^{\infty} \sum_{m=0}^{\infty} \frac{(t)^r}{r!} T_{m,k} \frac{\lambda b^{-\frac{r}{\beta}} \Gamma(1-\frac{r}{\beta}) \Gamma(\lambda(m+1)+\frac{r}{\beta})}{\Gamma(\lambda(m+1)+1)}. \tag{25}$$

4.4 Rényi Entropy

Entropy serves as a measure of the uncertainty variation of the random variable X. Given that X has the probability distribution function $f(x)$, the Rényi entropy is defined as follows:

$$H_\gamma(X) = \frac{1}{1-\gamma} \log\left(\int_0^{\infty} (f(x))^\gamma dx\right), \quad \gamma \neq 1 \tag{26}$$

© 2025 NSP
Natural Sciences Publishing Cor.

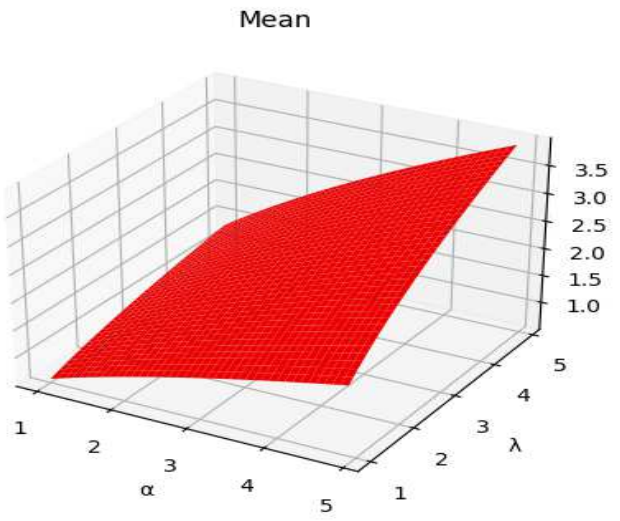

Mean

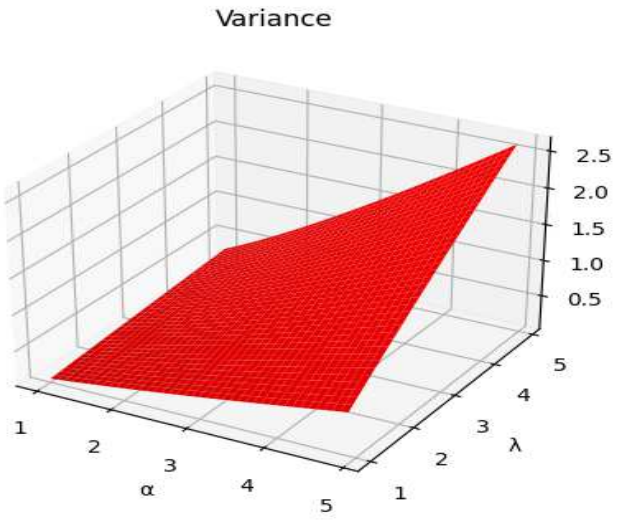

Variance

Fig. 5: Plot 3D of the mean and the variance for fixed value of $\beta = 2$ and $b = 2$

Suppose X has the probability density function $f(x)$ as given in (6). Then, one can calculate the Rényi entropy as:

$$H_\gamma(X) = \frac{1}{1-\gamma}\log\left\{\int_0^\infty \left(\frac{\lambda\beta}{b}\frac{\alpha\log(\alpha)}{(a-1)(\alpha+1)^2}\right)^\gamma x^{-\gamma(\beta+1)}\left(1+\frac{x^{-\beta}}{b}\right)^{-\gamma(\lambda+1)}\alpha^{\gamma\left(1+\frac{x^{-\beta}}{b}\right)^{-\lambda}}\left(1-\frac{\alpha^{\left(1+\frac{x^{-\beta}}{b}\right)^{-\lambda}}}{\alpha+1}\right)^{-2\gamma} dx\right\} \tag{27}$$

The Rényi entropy of the distribution can then be expressed as:

$$H_\gamma(X) = \frac{1}{1-\gamma}\log\left\{\left(\frac{\lambda\beta}{b}\frac{\alpha\log(\alpha)}{(a-1)(\alpha+1)^2}\right)^\gamma \int_0^\infty \sum_{m=0}^{\infty}\sum_{k=0}^{\infty}\frac{(k+1)(\gamma+k)^m(\log(\alpha))^m}{(\alpha+1)^k m!}x^{-\gamma(\beta+1)}\left(1+\frac{x^{-\beta}}{b}\right)^{-m\lambda-\gamma(\lambda+1)} dx\right\} \tag{28}$$

Utilizing the transformation in (16), we arrive at:

© 2025 NSP
Natural Sciences Publishing Cor.

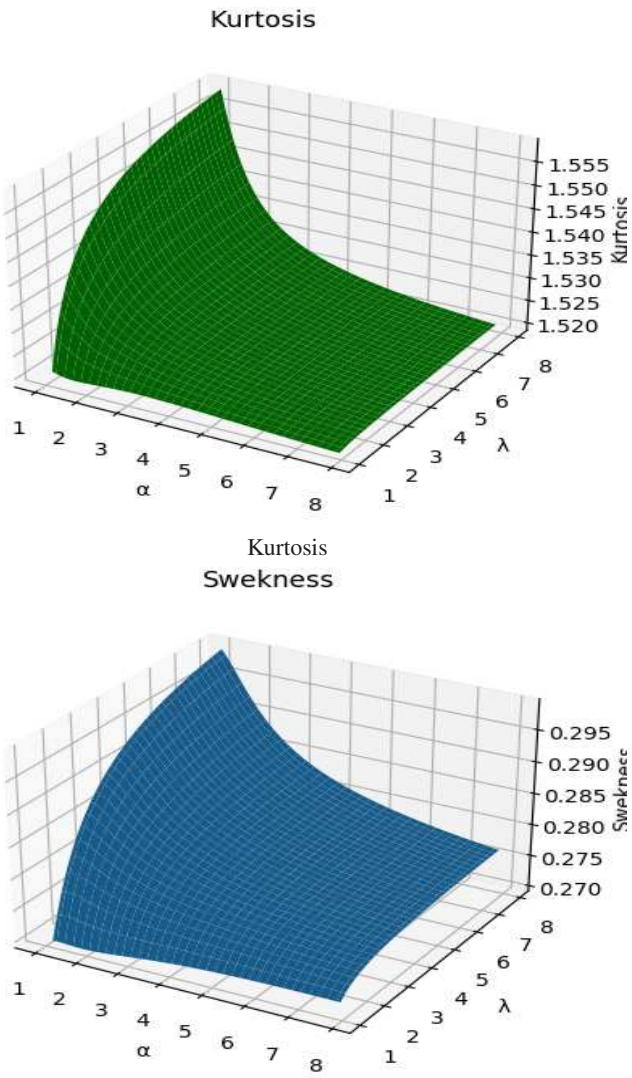

Kurtosis

Swekness

Fig. 6: Plot 3D of the kurtosis and the swekness for fixed value of $\beta = 2$ and $b = 2$

$$H_\gamma(X) = \frac{1}{1-\gamma}\log\left\{\left(\frac{\lambda\beta}{b}\frac{\alpha\log(\alpha)}{(a-1)(\alpha+1)^2}\right)^\gamma \sum_{m=0}^{\infty}\sum_{k=0}^{\infty} J_{k,m}\int_0^1 (1-y)^{\frac{(\beta+1)(\gamma+1)}{\beta}} y^{m\lambda+\gamma(\lambda+1)+\frac{(\beta+1)(\gamma+1)}{\beta}-2}dy\right\}$$

Hence, the Rényi entropy of the MAPT-IPL distribution is given by:

$$H_\gamma(X) = \frac{1}{1-\gamma}\log\left\{\left(\frac{\lambda\beta}{b}\frac{\alpha\log(\alpha)}{(a-1)(\alpha+1)^2}\right)^\gamma \sum_{m=0}^{\infty}\sum_{k=0}^{\infty} J_{k,m}B\left(1-\frac{(\beta+1)(\gamma+1)}{\beta};m\lambda+\gamma(\lambda+1)+\frac{(\beta+1)(\gamma+1)}{\beta}-1\right)\right\}$$

where

$$J_{k,m} = \frac{(k+1)(\gamma+k)^m(\log(\alpha))^m}{(\alpha+1)^k m!}\times\frac{1}{\beta}b^{1-\frac{(\beta+1)(\gamma+1)}{\beta}} \tag{29}$$

$B(.,.)$ denotes the beta function.

© 2025 NSP
Natural Sciences Publishing Cor.

4.5 Residual Life and Reversed Failure Rate Function

The r-th moment of the residual life (RL) of the random variable X is defined as follows:

$$R_r(t) = E\left((X-t)^r \,|\, X > t\right) = \frac{1}{1-F(t)} \int_t^{\infty} (x-t)^r f(x)\, dx, \quad r \geq 1$$

Here, $E(....)$ denotes the expected value, Ft represents the cumulative distribution function (CDF) of X evaluated at t, and f$x$is the probability density function (PDF) of X. The integral calculates the average of the r-th power of the remaining lifetime xt for units that have survived past t

Using (9) and applying the binomial expansion of $(x-t)^r$, we obtain:

$$\begin{aligned} R_r(t) &= \frac{1}{1-F(t)} \sum_{v=0}^{r} \binom{r}{v} (-t)^{r-v} \int_t^{\infty} x^r f(x)\, dx \\ &= \frac{1}{1-F(t)} \sum_{v=0}^{r} \sum_{m=0}^{\infty} T_{m,k} \binom{r}{v} (-t)^{r-v} \int_t^{\infty} x^r g(x;(m+1)\lambda, b, \beta)\, dx \\ &= \frac{1}{1-F(t)} \sum_{v=0}^{r} \sum_{m=0}^{\infty} T_{m,k} \binom{r}{v} (-t)^{r-v} \int_t^{\infty} \frac{(m+1)\lambda\beta}{b} x^{r-\beta-1} \left(1+\frac{x^{-\beta}}{b}\right)^{-(m+1)\lambda-1} dx \end{aligned} \tag{30}$$

where $g(x;(m+1)\lambda, b, \beta)$ is the PDF of the Inverse Power Lomax distribution.

Using the transformation:

$$u = \left(1+bx^{\beta}\right)^{-1}, \tag{31}$$

we get

$$du = -b\beta x^{\beta-1}\left(1+bx^{\beta}\right)^{-2} dx \quad \text{and} \quad x = \left(\frac{1}{b}\right)^{\frac{1}{\beta}} (1-u)^{\frac{1}{\beta}}\, u^{-\frac{1}{\beta}}.$$

By substituting (31) into equation (30) and applying the incomplete beta function integration, we have:

$$R_r(t) = \frac{1}{1-F(t)} \sum_{v=0}^{r} \sum_{m=0}^{\infty} T_{m,k} \binom{r}{v} (-t)^{r-v} (m+1)\lambda b^{-\frac{r}{\beta}} B\left[\left(\frac{1}{1+bt^{\beta}}\right), \left(1-\frac{r}{\beta}\right), \left((m+1)\lambda+\frac{r}{\beta}\right)\right] \tag{32}$$

where

$$\frac{1}{1-F(t)} = \frac{(\alpha-1)\left(1+\alpha-\alpha^{\left(1+\frac{t^{-\beta}}{b}\right)^{-\lambda}}\right)}{(\alpha-1)\left(1+\alpha-\alpha^{\left(1+\frac{t^{-\beta}}{b}\right)^{-\lambda}}\right) - \alpha^{\left(1+\frac{t^{-\beta}}{b}\right)^{-\lambda}} + 1}$$

and $B[.,.,.]$ is the incomplete beta function. The mean residual life, also known as the mean remaining life, is obtained by setting $r = 1$ in (32). The mean residual life is crucial in various fields such as industrial reliability, biomedical science, life insurance, and demography.

Conversely, the reversed residual life can be defined as the conditional random variable $t - X | X \leq t$, which denotes the time elapsed from the failure of a component given that its life is less than or equal to t. The n-th moment of the reversed residual life is given by:

$$\varepsilon_r(t) = \frac{1}{F(t)} \int_0^t (x-t)^r f(x) dx.$$

Applying the binomial series and using PDF (9), the n-th moment of the reversed residual life IPL distribution is:

$$\varepsilon_r(t) = \frac{1}{F(t)} \sum_{v=0}^{r} \sum_{m=0}^{\infty} T_{m,k} \binom{r}{v} (-t)^{r-v} \int_0^t \frac{(m+1)\lambda\beta}{b} x^{r-\beta-1} \left(1+\frac{x^{-\beta}}{b}\right)^{-(m+1)\lambda-1} dx \tag{33}$$

© 2025 NSP
Natural Sciences Publishing Cor.

Using the transformation:

$$u = \left(1 + \frac{x^{-\beta}}{b}\right)^{-1}, \tag{34}$$

we obtain

$$du = \frac{1}{b}\beta x^{-\beta-1}\left(1 + \frac{x^{-\beta}}{b}\right)^{-2} dx.$$

By substituting (34) into equation (33) and applying the incomplete beta function integration, we get:

$$\varepsilon_r(t) = \frac{1}{F(t)} \sum_{v=0}^{r} \sum_{m=0}^{\infty} T_{m,k} \binom{r}{v} (-t)^{r-v} (m+1)\lambda b^{-\frac{r}{\beta}} B\left[\left(1 + \frac{x^{-\beta}}{b}\right)^{-1}, \left(1 - \frac{r}{\beta}\right), \left((m+1)\lambda + \frac{r}{\beta}\right)\right] \tag{35}$$

Setting $r = 1$ in the r-th moment of the reversed RL (Equation (35)) provides the mean reversed residual life. This represents the average time a unit has spent waiting since its failure, given that it failed before time t. It's also known as the mean waiting time or mean inactivity time.

4.6 Order Statistics

Order statistics find wide applications in statistics, such as nonparametric statistics, life testing, quality control, and reliability analysis. Let $X_1, \ldots, X_n$ be a random sample drawn from the MAPT-IPL distribution, with cumulative distribution function (CDF) and probability density function (PDF) given by equations (6) and (3) respectively. Denote the order statistics of $X_1, \ldots, X_n$ as $X_{(1)}, \ldots, X_{(n)}$. The PDF of the ith order statistic, $X_{(i)}$, is then expressed as:

$$\begin{aligned} f_{X_{(i)}}(x) &= \frac{f(x)}{B(i, n-i+1)} F^{i-1}(x)\left[1 - F(x)\right]^{n-i} \\ &= \frac{f(x)}{B(i, n-i+1)} \sum_{k=0}^{n-i} \binom{n-i}{k} (-1)^k F^{k+i-1}(x) \\ &= \frac{1}{B(i, n-i+1)} \sum_{k=0}^{n-i} \binom{n-i}{k} (-1)^k f(x) F^{k+i-1}(x) \end{aligned} \tag{36}$$

where $B(\cdot,\cdot)$ represents the beta function.
Utilizing equations (6) and (3), we derive:

$$f(x)F^{k+i-1}(x) = \frac{\lambda\beta}{b} \frac{\alpha \log(\alpha)}{\left(a^2-1\right)^{k+i}(\alpha+1)} x^{-\beta-1}\left(1 + \frac{x^{-\beta}}{b}\right)^{-\lambda-1} \alpha^{\left(1+\frac{x^{-\beta}}{b}\right)^{-\lambda}} \left(1 - \frac{\alpha^{\left(1+\frac{x^{-\beta}}{b}\right)^{-\lambda}}}{\alpha+1}\right)^{-k-i-1} \left(\alpha^{\left(1+\frac{x^{-\beta}}{b}\right)^{-\lambda}} - 1\right)^{k+i-1}$$

By employing a power series expansion, we obtain:

$$f(x)F^{k+i-1}(x) = \frac{\lambda\beta}{b} \frac{\alpha \log(\alpha)}{(\alpha^2-1)^{k+i}(\alpha+1)} \sum_{m=0}^{\infty} \sum_{d=0}^{k+i-1} \sum_{p=0}^{\infty} (-1)^{k+i-1-d} \binom{k+i-1}{d} \frac{(p+1)(p+d+1)^m (\log(\alpha))^m}{m!(\alpha+1)^p} x^{-\beta-1}\left(1 + \frac{x^{-\beta}}{b}\right)^{-\lambda(m+1)-1} \tag{37}$$

Substituting equation (37) into equation (36), the PDF of $X_{(i)}$ simplifies to:

$$f_{X_{(i)}}(x) = \sum_{k=0}^{n-i} \sum_{m=0}^{\infty} \sum_{d=0}^{k+i-1} \sum_{p=0}^{\infty} M_{k,m} \times g\left(x; (m+1)\lambda, b, \beta\right),$$

where $g(x; (m+1)\lambda, b, \beta)$ represents the PDF of the Inverse Power Lomax distribution with scale parameter $(m+1)\lambda$ and shape parameter β, and

$$M_{k,m} = (-1)^{2k+i-1-d} \binom{n-i}{k} \binom{k+i-1}{d} \frac{\alpha (\log(\alpha))^{m+1} (p+1)(p+d+1)^m}{(m+1)!(\alpha+1)^{p+1}(\alpha^2-1)^{k+i}} \frac{1}{B(i, n-i+1)}$$

© 2025 NSP
Natural Sciences Publishing Cor.

5 Parameters estimation

In this section, we employ the method of maximum likelihood to derive estimates for the unknown parameters characterizing the MAPT-IPL distribution. We start by considering a random sample of size n drawn from the MAPT-IPL distribution, for which the PDF is defined by equation (6). From this, we proceed to formulate the log-likelihood function.

The likelihood function, denoted by $L(\alpha,\beta,b,\lambda)$, is constructed as the product of individual probability densities for each observation, where $f(x_k)$ represents the probability density function for each observation x_k:

$$L(\alpha,\beta,b,\lambda)=\prod_{k=1}^{n} f(x_k). \tag{38}$$

This likelihood function can be expressed as follows:

$$L(\alpha,\beta,b,\lambda)=\left(\frac{\lambda\beta}{b}\frac{\alpha\log(\alpha)}{(a-1)}\right)^{n}\prod_{k=1}^{n}\left\{x_k^{-\beta-1}\left(1+\frac{x_k^{-\beta}}{b}\right)^{-\lambda-1}\frac{\alpha^{\left(1+\frac{x_k^{-\beta}}{b}\right)^{-\lambda}}}{\left(1+\alpha-\alpha^{\left(1+\frac{x_k^{-\beta}}{b}\right)^{-\lambda}}\right)^{2}}\right\}.$$

The log-likelihood function, denoted as $l(\alpha,\beta,b,\lambda)$, is defined as the natural logarithm of the likelihood function:

$$l(\alpha,\beta,b,\lambda)=\log\left[L(\alpha,\beta,b,\lambda))\right], \tag{39}$$

so we obtain :

$$\begin{aligned} l(\alpha,\beta,b,\lambda)=n\log\left(\frac{\lambda\beta}{b}\frac{\alpha\log(\alpha)}{(a-1)}\right)-(\beta+1)\sum_{k=1}^{n}\log(x_k)+(\lambda+1)\sum_{k=1}^{n}\log\left(1+\frac{x_k^{-\beta}}{b}\right)+\log(\alpha)\sum_{k=1}^{n}\left(1+\frac{x_k^{-\beta}}{b}\right)^{-\lambda}\\ -2\sum_{k=1}^{n}\log\left(1+\alpha-\alpha^{\left(1+\frac{x_k^{-\beta}}{b}\right)^{-\lambda}}\right) \end{aligned} \tag{40}$$

In order to obtain the maximum likelihood estimates (MLEs) of the parameters α, β, b, and λ, denoted as $\hat{\alpha}$, $\hat{\beta}$, $\hat{b}$, and $\hat{\lambda}$ respectively, we maximize the objective function in equation (40) with respect to each of these parameters. Alternatively, one can solve the following set of normal equations simultaneously:

$$\frac{\partial l}{\partial\alpha}=\frac{n}{\alpha}+\frac{n}{\alpha\log(\alpha)}-\frac{n}{\alpha-1}+\frac{1}{\alpha}\sum_{k=1}^{n}\left(1+\frac{x_k^{-\beta}}{b}\right)^{-\lambda}-2\sum_{k=0}^{n}\frac{1-\left(1+\frac{x_k^{-\beta}}{b}\right)^{-\lambda}\alpha^{\left(1+\frac{x_k^{-\beta}}{b}\right)^{-\lambda}-1}}{1+\alpha-\alpha^{\left(1+\frac{x_k^{-\beta}}{b}\right)^{-\lambda}}}=0, \tag{41}$$

$$\frac{\partial l}{\partial\beta}=\frac{n}{\beta}-\sum_{k=1}^{n}\log(x_k)-\frac{(\lambda+1)\beta}{b}\sum_{k=1}^{n}\frac{x_k^{-\beta-1}}{1+\frac{x_k^{-\beta}}{b}}+\frac{\lambda\beta\log(\alpha)}{b}\sum_{k=0}^{n}x_k^{-\beta-1}\left(1+\frac{x_k^{-\beta}}{b}\right)^{-\lambda-1}+\frac{2\lambda\beta\log(\alpha)}{b}\sum_{k=0}^{n}\frac{x_k^{-\beta-1}\left(1+\frac{x_k^{-\beta}}{b}\right)^{-\lambda-1}\alpha^{\left(1+\frac{x_k^{-\beta}}{b}\right)^{-\lambda}}}{1+\alpha-\alpha^{\left(1+\frac{x_k^{-\beta}}{b}\right)^{-\lambda}}}=0, \tag{42}$$

$$\frac{\partial l}{\partial b}=-\frac{n}{b}-\frac{(\lambda+1)}{b^2}\sum_{k=1}^{n}\frac{x_k^{-\beta}}{1+\frac{x_k^{-\beta}}{b}}+\frac{\lambda\log(\alpha)}{b^2}\sum_{k=0}^{n}x_k^{-\beta}\left(1+\frac{x_k^{-\beta}}{b}\right)^{-\lambda-1}+\frac{2\lambda\log(\alpha)}{b^2}\sum_{k=0}^{n}\frac{x_k^{-\beta}\left(1+\frac{x_k^{-\beta}}{b}\right)^{-\lambda-1}\alpha^{\left(1+\frac{x_k^{-\beta}}{b}\right)^{-\lambda}}}{1+\alpha-\alpha^{\left(1+\frac{x_k^{-\beta}}{b}\right)^{-\lambda}}}=0, \tag{43}$$

© 2025 NSP
Natural Sciences Publishing Cor.

$$\frac{\partial l}{\partial \lambda} = \frac{n}{\lambda} + \sum_{k=1}^{n} \log\left(1+\frac{x_k^{-\beta}}{b}\right) - \log(\alpha)\sum_{k=1}^{n}\left(1+\frac{x_k^{-\beta}}{b}\right)^{-\lambda}\log\left(1+\frac{x_k^{-\beta}}{b}\right) - 2\log(\alpha)\sum_{k=0}^{n}\frac{\left(1+\frac{x_k^{-\beta}}{b}\right)^{-\lambda}\log\left(1+\frac{x_k^{-\beta}}{b}\right)\alpha^{\left(1+\frac{x_k^{-\beta}}{b}\right)^{-\lambda}}}{1+\alpha-\alpha^{\left(1+\frac{x_k^{-\beta}}{b}\right)^{-\lambda}}} = 0, \tag{44}$$

These equations involve partial derivatives of the log-likelihood function $l(\alpha,\beta,b,\lambda)$ with respect to each parameter. Despite the availability of these equations, it's worth noting that closed-form solutions do not exist for them (equations (41)–(44)). Therefore, obtaining the MLEs in this scenario necessitates the application of numerical techniques. Various numerical methods, such as gradient descent or Newton's method, can be employed for this purpose.

6 Simulation Study

In this section, we conducted a simulation study to assess the performance of maximum likelihood estimators (MLEs) under varying sample sizes and parameter values. The study aimed to evaluate the accuracy and reliability of the estimators in estimating the parameters of the MAPT-IPL distribution.

6.1 Simulation Setup

The simulation process involved generating random samples from the MAPT-IPL distribution with predefined parameter values. Three sets of parameters were considered:

- $\alpha = 2 \quad \beta = 3 \quad b = 1 \quad \lambda = 0.5$
- $\alpha = 4 \quad \beta = 0.5 \quad b = 12 \quad \lambda = 0.5$
- $\alpha = 0.5 \quad \beta = 1 \quad b = 2.5 \quad \lambda = 0.5$

These parameter combinations were chosen to represent a diverse range of distribution shapes and characteristics.

For each parameter set, random samples of different sizes (ranging from 25 to 500) were generated. The sample sizes considered were: 25, 50, 100, 200, 300, 400, and 500. For each sample size, we performed 2000 replicates. The MLEs for the parameters α, β, b, and λ were computed for each replicate.

6.2 Metrics Calculation

To assess the accuracy and precision of the estimators, we calculated the bias (BAIS) and root mean square error (RMSE) of the estimators for each sample size. The bias measures the difference between the expected value of the estimator and the true parameter value, while the RMSE provides an indication of the estimator's variability and overall error.

6.3 Simulation Results

The simulation results, presented in Tables 1, 2, and 3, provide insights into the performance of the MLEs under different scenarios. The tables display the MLEs, BAIS, and RMSE for each parameter and sample size combination. Analysis of these results allows us to evaluate the impact of sample size on estimation accuracy and identify any patterns or trends across different parameter values.

6.4 Interpretation of Results

As the sample size increases, we observe a consistent decrease in both the bias and RMSE of the estimators. This indicates that the estimators become more accurate and precise with larger sample sizes. Specifically, a smaller bias suggests that the estimators are closer to the true parameter values on average, while a lower RMSE indicates a reduction in the variability of the estimators around the true values. Consequently, the MLEs exhibit improved performance with increasing sample sizes, demonstrating their consistency and reliability in estimating the parameters of the MAPT-IPL distribution.

Overall, the simulation study serves as a comprehensive analysis of the performance of MLEs in estimating the parameters of the MAPT-IPL distribution, providing valuable insights for practitioners and researchers in reliability analysis and statistical modeling.

© 2025 NSP
Natural Sciences Publishing Cor.

Table 1: The MLEs, BAIS, RMSE of the parameters $\alpha = 2$, $\beta = 3$, $b = 1$ and $\lambda = 0.5$ for different sample sizes

Sample Size	Parameters	MLEs	BAIS	RMSE
	α	3.535757	1.535757	6.520062
25	β	3.341697	0.341697	0.923350
	b	11.868686	10.868686	73.096877
	λ	0.524013	0.024013	0.378326
	α	2.492968	0.492968	2.526116
50	β	3.707437	0.707437	1.785797
	b	2.120404	1.120404	4.931176
	λ	0.490377	-0.009623	0.229254
	α	2.189236	0.189236	2.571163
100	β	3.469265	0.469265	1.290217
	b	1.075800	0.075800	1.412599
	λ	0.494059	-0.005941	0.202407
	α	2.777120	0.777120	3.227292
200	β	3.271394	0.271394	0.747653
	b	1.464986	0.464986	2.360385
	λ	0.452181	-0.047820	0.132061
	α	2.330242	0.330242	3.124408
300	β	3.246371	0.246371	0.521520
	b	1.218709	0.218709	2.091602
	λ	0.494791	-0.005209	0.111725
	α	2.206878	0.206878	1.496763
400	β	3.104531	0.104531	0.301546
	b	1.199070	0.199070	1.230551
	λ	0.493167	-0.006833	0.095951
	α	2.245440	0.245440	1.718610
500	β	3.148235	0.148235	0.352376
	b	1.142184	0.142184	1.264033
	λ	0.476994	-0.023006	0.086673

© 2025 NSP
Natural Sciences Publishing Cor.

Table 2: The MLEs, BAIS, RMSE of the parameters $\alpha = 4$, $\beta = 0.5$, $b = 12$ and $\lambda = 0.5$ for different sample sizes

Sample Size	Parameters	MLEs	BAIS	RMSE
	α	9.139774	5.139774	32.380736
25	β	0.535358	0.035358	0.126384
	b	9.279311	-2.720689	12.456966
	λ	0.602368	0.102367	0.302546
	α	4.506939	0.506938	5.781510
50	β	0.567641	0.067640	0.145702
	b	9.597977	-2.402023	9.865411
	λ	0.647749	0.147749	0.442364
	α	5.479764	1.479764	9.151007
100	β	0.541346	0.041346	0.106078
	b	11.839593	-0.160407	13.582216
	λ	0.534901	0.034901	0.181589
	α	4.952801	0.952801	5.778503
200	β	0.560582	0.060582	0.287411
	b	12.993930	0.993930	14.075140
	λ	0.566840	0.066840	0.331122
	α	4.519814	0.519814	5.884703
300	β	0.525274	0.025274	0.080680
	b	12.086284	0.086284	13.821552
	λ	0.531758	0.031758	0.189271
	α	4.155074	0.155074	2.801868
400	β	0.504353	0.004353	0.027507
	b	12.474893	0.474893	9.341244
	λ	0.530542	0.030542	0.125764
	α	4.016758	0.016757	3.938610
500	β	0.568461	0.068461	0.164675
	b	12.343453	0.343453	16.471291
	λ	0.505781	0.005781	0.157793

© 2025 NSP
Natural Sciences Publishing Cor.

Table 3: The MLEs, BAIS, RMSE of the parameters $\alpha = 0.5$, $\beta = 1$, $b = 2.5$ and $\lambda = 0.5$ for different sized samples

Sample Size	Parameters	MLEs	BAIS	RMSE
	α	0.941015	0.441015	1.369947
25	β	3.562908	2.562908	6.974768
	b	6.219616	3.719616	9.931237
	λ	0.442011	-0.057989	0.154157
	α	0.737925	0.237925	0.991106
50	β	2.028074	1.028074	2.734240
	b	4.824441	2.324441	8.452318
	λ	0.393574	-0.106426	0.255895
	α	0.646768	0.146768	0.651819
100	β	1.074214	0.074214	0.212988
	b	4.306292	1.806292	7.298033
	λ	0.475084	-0.024916	0.094411
	α	0.523312	0.023312	0.319747
200	β	1.223240	0.223240	0.755847
	b	3.216535	0.716535	3.438333
	λ	0.470132	-0.029868	0.120840
	α	0.615645	0.115645	0.565138
300	β	1.087400	0.087400	0.272147
	b	4.413129	1.913129	7.137540
	λ	0.488444	-0.011556	0.114040
	α	0.542136	0.042136	0.356814
400	β	1.123630	0.123630	0.410604
	b	3.339424	0.839424	3.964073
	λ	0.470363	-0.029637	0.095278
	α	0.549753	0.049753	0.276141
500	β	1.074852	0.074852	0.172614
	b	3.263812	0.763812	2.780065
	λ	0.464362	-0.035638	0.067006

© 2025 NSP
Natural Sciences Publishing Cor.

7 Application

In this section, we delve into the comprehensive evaluation of the proposed MAPT-IPL distribution through rigorous data analysis. The performance assessment was conducted utilizing three distinct datasets carefully selected to represent a diverse range of real-world scenarios. Each dataset was meticulously curated to capture various complexities and nuances prevalent in practical applications.

Furthermore, to establish a robust benchmark for comparison, the performance of the MAPT-IPL distribution was juxtaposed against several existing competing models. These included :

–Modified Alpha Power Transformed Weibull distribution (MAPTW) [56]
–Alpha power transformed generalized exponential distribution (APTGE) [59]
–Alpha Power Transformed Inverse Lomax (APTIL) [53]

–Alpha Power Transformed Lomax (APTL) [54]

–Inverse Power Lomax (IPL) [47]

renowned distributions known for their versatility and applicability in diverse domains. (See Table 4)

Parameter estimation, an essential component in statistical modeling, was conducted using the Maximum Likelihood Estimation (MLE) method. This robust and widely recognized approach ensures the optimal fitting of parameters to the observed data, enabling accurate inference and reliable predictions.To assess the variability and precision of the estimated parameters, the standard errors and confidence intervals were calculated. The standard errors were derived from the Fisher information matrix, a well-established method for quantifying estimation accuracy. For the confidence intervals, a 95% confidence level was utilized to provide a balanced perspective on parameter uncertainty.As all parameters of the models distribution are theoretically constrained to be positive, adjustments were made to ensure non-negativity in cases where the lower bounds of the confidence intervals included negative values. Specifically, any negative lower bounds were replaced with zero, resulting in modified intervals that ranged from 0 to the non-negative upper bound of the original interval.To enhance the interpretability and visual presentation of the results, MATLAB, a versatile computational software, was employed. This facilitated the generation of detailed plots that illustrate the distribution's goodness-of-fit and its capability to capture the underlying data structure effectively. This meticulous approach to parameter estimation and interval construction not only underscores the reliability of the proposed MAPT-IPL distribution but also ensures its adherence to theoretical constraints. By addressing both statistical and computational aspects, this analysis strengthens the foundation for the applicability of the MAPT-IPL distribution in modeling real-world datasets.

Dataset I:

The first dataset under review concerns the remission times, measured in months, of a random sample comprising 128 patients diagnosed with bladder cancer, as documented in [60]. This dataset has also been analyzed in [54].This dataset presents a diverse array of remission times, reflecting the varying responses observed among patients following treatment. A brief overview of the dataset reveals a wide range of remission durations, spanning from relatively short periods to significantly longer intervals.

The remission times listed provide valuable insights into the effectiveness of treatments administered to bladder cancer patients. Understanding the distribution and characteristics of remission times is crucial for healthcare professionals and researchers alike in evaluating treatment outcomes and devising optimal patient care strategies.

In the subsequent analysis, this dataset will undergo thorough examination and comparison with other existing models to assess the performance and applicability of the proposed MAPT-IPL distribution. The observations from the dataset are presented in table 5:

To further explore the dataset, graphical analyses have been conducted. Figure 7 presents two key visual representations: the TTT-plot and the Kaplan-Meier (K-M) plot. These figures play a crucial role in understanding the

© 2025 NSP
Natural Sciences Publishing Cor.

Table 4: The PDFs of different competitive models

Distribution	PDF	Conditions
MAPTW	$\frac{\lambda\theta\log(\alpha)x^{\theta-1}e^{-\lambda x^{\theta}}\alpha^{2-e^{-\lambda x^{\theta}}}}{(\alpha-1)\left[1+\alpha-\alpha^{1-e^{-\lambda x^{\theta}}}\right]^2}$	$x>0,\ \alpha,\theta,\lambda>0,\alpha\neq 1$
APTGE	$\frac{\beta\lambda\log\alpha}{\alpha-1}\exp(-\lambda x)\left[1-\exp(-\lambda x)\right]^{\beta-1}\alpha^{[1-\exp-\lambda x]^{\beta}}$	$x>0,\ \alpha,\beta,\lambda>0,\ \alpha\neq 1$
APTIL	$\frac{\log(\alpha)}{\alpha-1}\frac{ab}{x^2}\left(1+\frac{b}{x}\right)^{-a-1}\alpha^{\left(1+\frac{b}{x}\right)^{-a}}$	$x>0,\alpha,a,b>0\alpha\neq 1$
APTL	$\frac{\alpha\log(\alpha)}{\alpha-1}\frac{\theta}{\beta}\left(1+\frac{x}{\beta}\right)^{-\theta-1}\alpha^{-\left(1+\frac{x}{\beta}\right)^{-\theta}}$	$x>0,\quad \alpha,\beta,\theta>0,\alpha\neq 1$
IPL	$\frac{\lambda\beta}{b}x^{-\beta-1}\left(1+\frac{x^{-\beta}}{b}\right)^{-\lambda-1}$	$x>0,\quad b,\beta,\lambda>0$

Table 5: Dataset I

0.08	3.36	8.37	1.46	7.87	2.83	16.62	7.59	3.88	26.31	9.47	5.06	3.52
2.09	6.76	12.02	4.40	11.64	4.33	43.01	10.66	5.32	0.81	14.24	7.09	4.98
3.48	12.07	2.02	5.85	17.36	5.49	1.19	15.96	7.39	2.62	25.82	9.22	6.97
4.87	21.73	3.31	8.26	1.40	7.66	2.75	36.66	10.34	3.82	0.51	13.80	9.02
6.94	2.07	4.51	11.98	3.02	11.25	4.26	1.05	14.83	5.32	2.54	25.74	13.29
8.66	3.36	6.54	19.13	4.34	17.14	5.41	2.69	34.26	7.32	3.70	0.50	0.40
13.11	6.93	8.53	1.76	5.71	79.05	7.63	4.23	0.90	10.06	5.17	2.46	2.26
23.63	8.65	12.03	3.25	7.93	1.35	17.12	5.41	2.69	14.77	7.28	3.64	3.57
0.20	12.63	20.28	4.50	11.79	2.87	46.12	7.62	4.18	32.15	9.74	5.09	2.23
22.69	2.02	6.25	18.10	5.62	1.26	10.75	5.34	2.64	14.76	7.26		

© 2025 NSP
Natural Sciences Publishing Cor.

dataset's statistical properties. The TTT-plot (Figure 7a) provides a diagnostic view of the dataset, helping to assess the goodness-of-fit for proposed models. Meanwhile, the Kaplan-Meier plot (Figure 7b) depicts the survival probabilities over time, offering a comprehensive view of remission trends within the sample. Together, these graphical tools enhance our ability to interpret the remission data and evaluate the efficacy of various models.

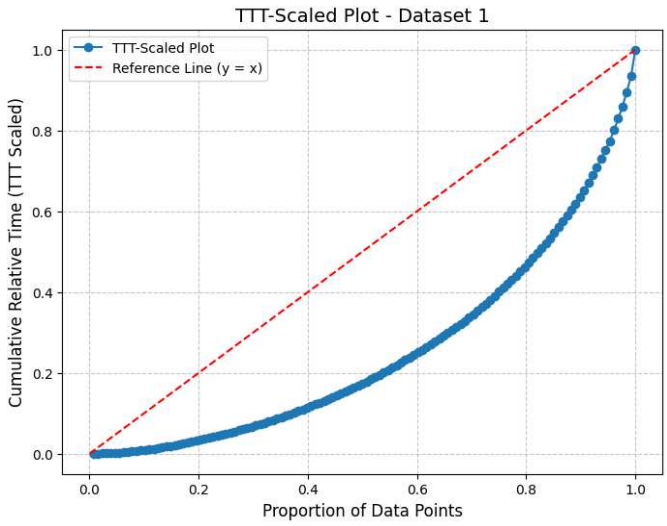

TTT-plot

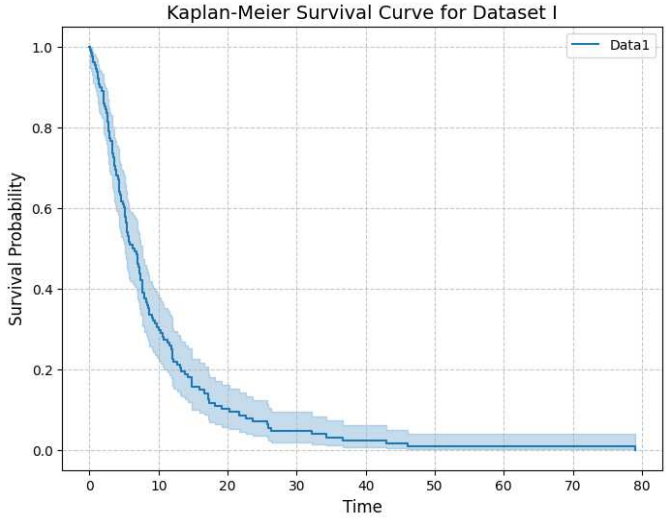

K-M plot

Fig. 7: Graphical representation of the TTT-scaled plot and Kaplan-Meier plot (Dataset I).

Table 7 provides a detailed summary of the estimated parameters for various models applied to Dataset I. Each model's parameters are presented alongside their standard errors and 95% confidence intervals, offering a robust statistical characterization of the dataset. This table is instrumental in comparing model performance and identifying the most suitable framework for analyzing remission times.

Further model comparisons are detailed in Table 6, which outlines the information criteria and additional statistics for Dataset I. Metrics such as AIC, BIC, and K-S statistics provide insights into the adequacy and performance of various models, enabling a rigorous evaluation. Finally, Figure **??** provide empirical PDFs and CDFs for Dataset I, while Figure 9 illustrates the hazard rate functions for the models and the Q-Q plot of the MAPT-IPL model.These visualizations collectively enrich our understanding of the dataset's distributional properties and model fit.

© 2025 NSP
Natural Sciences Publishing Cor.

Table 6: Information criteria and additional statistics for the hailing time data (Dataset I)

Model	$-\hat{l}$	AIC	CAIC	BIC	HQIC	W	K-S	K-S (p-value)
MAPT-IPL	**407.574**	**821.148**	**822.473**	**831.556**	**828.783**	**0.6874**	**0.2147**	**0.0001**
MAPTW	409.57	825.15	836.71	833.71	828.63	0.6874	0.2208	0.0001
APTGE	410.27	826.55	838.10	835.10	830.02	0.6874	0.2198	0.0001
APTIL	409.92	825.84	837.39	834.39	829.31	0.6874	0.2210	0.0001
APTL	409.38	826.77	827.09	838.17	831.40	0.6874	0.2242	0.0001
IPL	409.698	827.396	827.721	838.804	832.031	0.6874	0.2216	0.0001

Dataset II:

The dataset represents the estimated duration (in years) from the administration of growth hormone therapy until children reached the specified target age. This information is crucial for analyzing the impact of hormone treatments on childhood development, helping to assess how long it typically takes for the therapy to produce measurable results. The dataset was originally analyzed in [61] in their study of growth patterns under hormonal treatment. This dataset serves as an essential resource for studying growth trajectories in children receiving hormonal therapy. By examining these intervals, researchers can better assess the variability in response times and identify potential factors influencing treatment outcomes. Such analyses contribute to optimizing therapeutic strategies and improving patient care. The observations are presented in table 8.

Next, we present graphical representations of the dataset, starting with the TTT-plot and the Kaplan-Meier (K-M) plot, as shown in Figure 10. These plots provide further insights into the time-to-treatment (TTT) scaling and the survival distribution of the dataset.

In Table 9, we present the estimated values, standard errors, and confidence intervals for the parameters in the various models applied to Dataset II. These values are crucial for understanding the model performance and the uncertainty associated with each parameter estimate. Following this, Table 10 presents the information criteria and additional statistical measures, such as the Akaike Information Criterion (AIC) and Bayesian Information Criterion (BIC), for each model fitted to the data.

Subsequently, we present the empirical probability density functions (pdfs) and cumulative distribution functions (cdfs) for the different models, as shown in Figure 11.Finally, Figure **??** illustrates the hazard rate functions for the models and the Q-Q plot of the MAPT-IPL model. These plots offer a visual comparison of how each model fits the data and the resulting distribution.

Dataset III

The dataset analyzed in [59] consists of daily ozone measurements recorded in New York during the months of May to September in the year 1973. This dataset is particularly valuable for studying atmospheric conditions, seasonal trends, and potential environmental factors influencing ozone levels over this period. By examining these observations, researchers can gain insights into historical air quality patterns and their implications for environmental health and policy development. The observations are presented in table 11

Figures **??** provide graphical representations of the dataset using the TTT-plot and Kaplan-Meier (K-M) plot. These visualizations offer additional insights into time-to-treatment scaling and survival distributions.

In table 12, we present the estimated values, standard errors, and confidence intervals for the parameters in the various models applied to Dataset III. These values are crucial for understanding the model performance and the

© 2025 NSP
Natural Sciences Publishing Cor.

Table 7: Estimated values, standard errors, and confidence intervals for dataset I

Model	Parameter	Estimate	Standard Error	Confidence Interval (95%)
MAPT-IPL	α	1.9943	0.1012	[1.796, 2.192]
	β	1.9379	0.0897	[1.761, 2.115]
	b	0.0308	0.0053	[0.020, 0.041]
	λ	0.5407	0.0442	[0.454, 0.627]
MAPTW	α	1028	0.0018	[1027.96 , 1028.04]
	θ	0.1976	0.001	[0.178, 0.2172]
	λ	6.16	1.07	[4.06 , 8.25]
APTGE	α	0.0986	0.0016	[0.095, 0.10]
	β	1.3719	0.15	[1.761, 2.115]
	λ	0.0714	0.02	[0.032, 0.1106]
APTIL	α	1.22×10^{-4}	1.01	[-1.97 1.97]
	b	31.0690	0.36	[30.34 , 31.78]
	λ	1.4446	0.24	[0.97 , 1.91]
APTL	α	28.5400	0.12	[28.29 , 28.77]
	β	8.2720	1.34	[5.64 , 10.90]
	θ	2.8740	1.453	[0.032 , 5.71]
IPL	β	2.1727	0.81	[0.58 , 3.76]
	b	0.0080	0.1	]0 0.204]
	λ	0.5858	1.76	]0 , 4.03]

© 2025 NSP
Natural Sciences Publishing Cor.

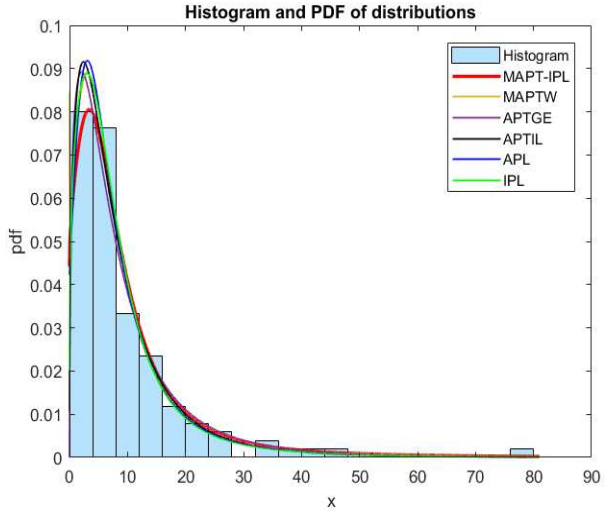

histogram and pdfs

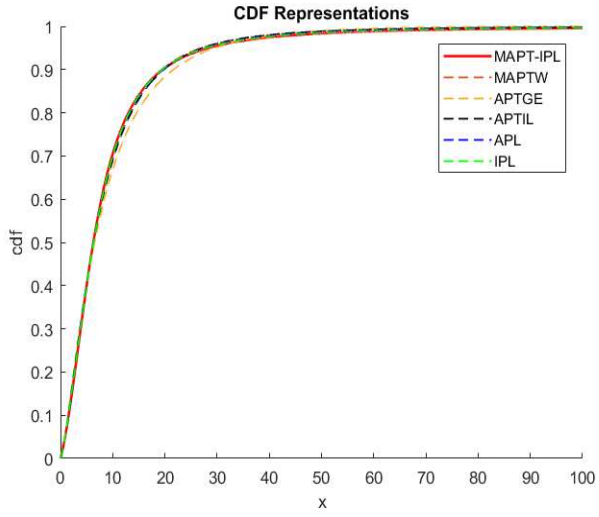

cdfs

Fig. 8: Graphical representation of the pdf and cdf (dataset I)

Table 8: Dataset II

2.15	2.20	2.55	2.56	2.63	2.74	2.81	2.90	3.05	3.41	3.43	3.43
3.84	4.16	4.18	4.36	4.42	4.51	4.60	4.61	4.75	5.03	5.10	5.44
5.90	5.96	6.77	7.82	8.00	8.16	8.21	8.72	10.40	13.20	13.70	

© 2025 NSP
Natural Sciences Publishing Cor.

Table 9: Estimated values, standard errors, and confidence intervals for dataset II

Model	Parameter	Estimate	Standard Error	Confidence Interval (95%)
MAPT-IPL	α	1.64	3.05	]0, 7.64]
	β	2.81	6.53	]0, 15.61]
	b	43.44	0.12	[43.19, 43.68]
	λ	1098.02	0.99	[1096.07, 1099.98]
MAPTW	α	3172.06	1.00	[3170.10, 3174.24]
	θ	0.3277	0.29	]0 , 0.89]
	λ	6.13	0.4471	[5.25, 7.00]
APTGE	α	0.2213	3.042	]0, 6.18]
	β	6.3690	0.61	[5.15 , 7.57]
	λ	0.3950	0.26	]0 , 0.90]
APTIL	α	2.49×10^{-4}	1.012	]0 , 1.98]
	b	2.17×10^{-2}	2.39	]0, 4.51]
	λ	521.20	0.0012	[521.18 521.22]
APTL	α	2.6754×10^{5}	1.00	$[\ 2.675455 \times 10^{5}\ ,\ 2.675456 \times 10^{5}\ ]$
	β	9.054	1.33	[6.44 ,11.66]
	θ	7.030	2.11	[2.87 , 11.18]
IPL	β	2.43	1.02	]0.43, 4.42]
	b	31.18	1.013	[29.19 33.16]
	λ	761.61	1.00	[759.65 763.57]

© 2025 NSP
Natural Sciences Publishing Cor.

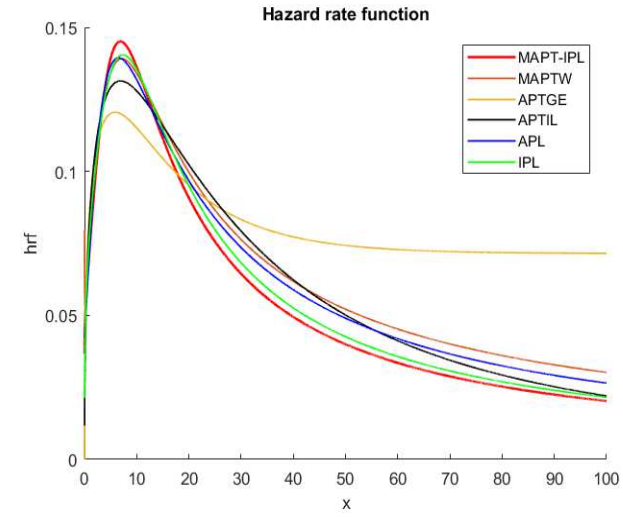

Illustration of hrf

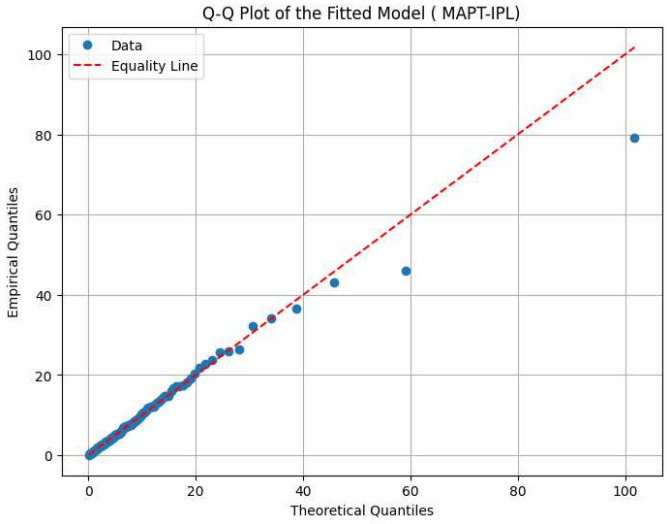

Q-Q plot

Fig. 9: Graphical representation of the hazard rate and Q-Q plot for MAPT-IPL (dataset I)

Table 10: Information criteria and additional statistics for the hailing time data (Dataset II)

Model	$-\hat{l}$	**AIC**	**CAIC**	**BIC**	**HQIC**	W	**K-S**	**K-S (p-value)**
MAPT-IPL	**77.53**	**160.06**	**168.29**	**165.39**	**162.21**	**0.8520**	**0.2264**	**0.1572**
MAPTW	80.49	166.98	174.64	171.64	168.59	0.8520	0.1755	0.1572
APTGE	78.62	163.24	170.91	167.91	164.86	0.8520	0.1870	0.1572
APTIL	78.24	162.48	170.14	167.14	164.09	0.8520	0.1993	0.1572
APTL	78.63	163.26	170.93	167.93	164.88	0.8520	0.1871	0.1572
IPL	77.72	161.45	169.11	166.11	163.06	0.8520	0.2291	0.1572

© 2025 NSP
Natural Sciences Publishing Cor.

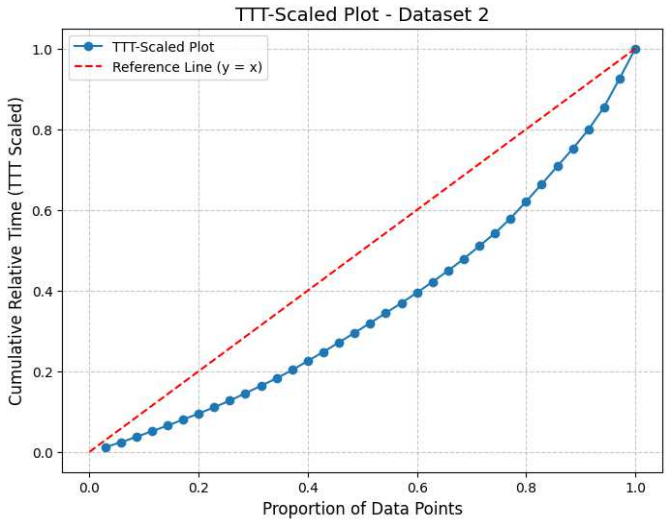

TTT-plot

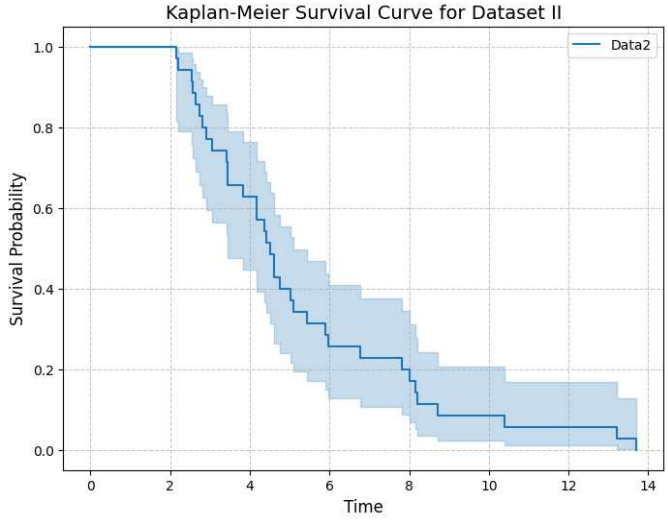

K-M plot

Fig. 10: Graphical representation of the TTT-scaled plot and Kaplan-Meier plot (Dataset II).

Table 11: Dataset III

41	36	12	18	28	23	19	8	7	16	11	14	18	14	34	6	30	11
1	11	4	32	23	45	115	37	29	71	39	23	21	37	20	12	13	135
49	32	64	40	77	97	97	85	10	27	7	48	35	61	79	63	16	80
108	20	52	82	50	64	59	39	9	16	78	35	66	122	89	110	44	28
65	22	59	23	31	44	21	9	45	168	73	76	118	84	85	96	78	73
91	47	32	20	23	21	24	44	21	28	9	13	46	18	13	24	16	13
23	36	7	14	30	14	18	20										

uncertainty associated with each parameter estimate. Following this, Table 13 presents the information criteria and additional statistical measures, such as the Akaike Information Criterion (AIC) and Bayesian Information Criterion (BIC), for each model fitted to the data. Finally, Figure 14 provide empirical PDFs and CDFs for Dataset III, while

© 2025 NSP
Natural Sciences Publishing Cor.

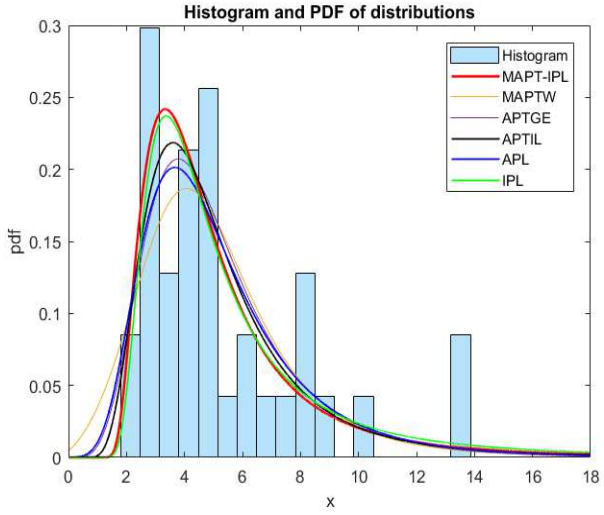

histogram and pdfs

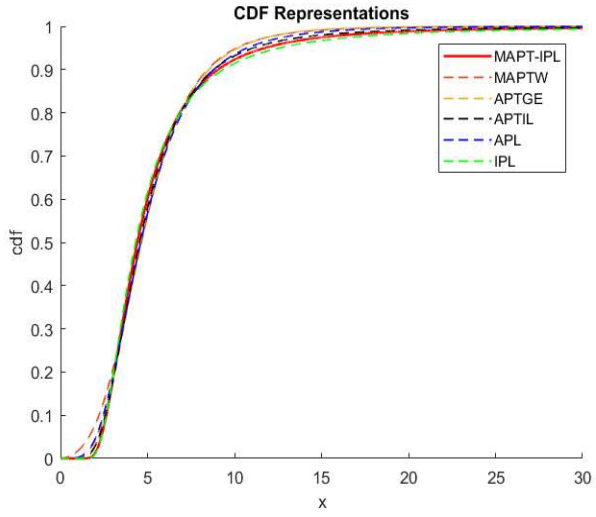

cdfs

Fig. 11: Graphical representation of the pdf and cdf (dataset II)

Figure ?? illustrates the hazard rate functions for the models and the Q-Q plot of the MAPT-IPL model.These visualizations collectively enrich our understanding of the dataset's distributional properties and model fit.

8 Discussion

The implementation of the MAPT-IPL distribution on three real-world datasets has yielded valuable insights, supported by comprehensive analyses of density curves, information criteria, and other key metrics. This discussion highlights the outstanding performance of the MAPT-IPL model compared to its competitors, specifically MAPTW, APTGE, APTIL, APTL, and IPL.Figures ??, 11, and 14 illustrate the estimated density functions overlaid on the corresponding histograms of the datasets. These figures offer a clear visual demonstration of the MAPT-IPL distribution's ability to align closely with the data. The superior fit of the MAPT-IPL model is evident in its capacity to accurately capture the peaks, tails, and overall structure of the observed data, surpassing the performance of alternative models. Quantitative evaluations further substantiate the advantages of the MAPT-IPL distribution. The values of widely recognized information criteria—AIC,

© 2025 NSP
Natural Sciences Publishing Cor.

Table 12: Estimated values, standard errors, and confidence intervals for dataset III

Model	Parameter	Estimate	Standard Error	Confidence Interval (95%)
MAPT-IPL	α	0.0097	2.50	]0, 4.997]
	β	2.17	0.29	[1.30, 2.73]
	b	1.55×10^{-5}	6.64	]0, 13.01]
	λ	0.919	2.01	]0, 4.8586]
MAPTW	α	0.407	0.1012	[0.20, 0.60]
	θ	1.702	0.0897	[1.53,1.87]
	λ	6.18×10^{-4}	0.0442	[0.454, 0.627]
APTGE	α	0.4808	4.74	]0, 9.78]
	β	1.9266	6.00	]0, 13.68]
	λ	0.0302	0.388	]0, 0.7906]
APTIL	α	10^{-6}	6.35	]0, 12.44]
	b	162	1.002	[160, 164]
	a	1.69	16.18	]0, 33.41]
APTL	α	95.26	0.021	[95.22 , 95.30]
	β	46.01	0.242	[45.54 , 46.49]
	θ	3.59	4.243	]0 ,11.91]
IPL	β	2.2705	19.66	]0 , 40.32]
	b	2.45×10^{-4}	1.6746	]0 , 3.28]
	λ	0.7432	11.68	]0 , 23.24]

© 2025 NSP
Natural Sciences Publishing Cor.

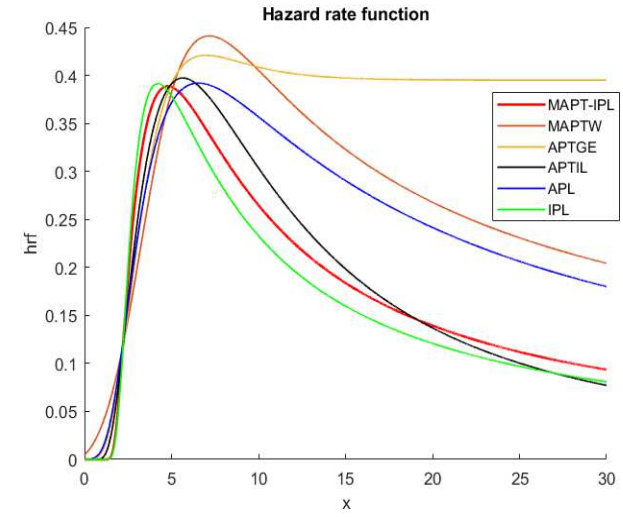

Illustration of hrf

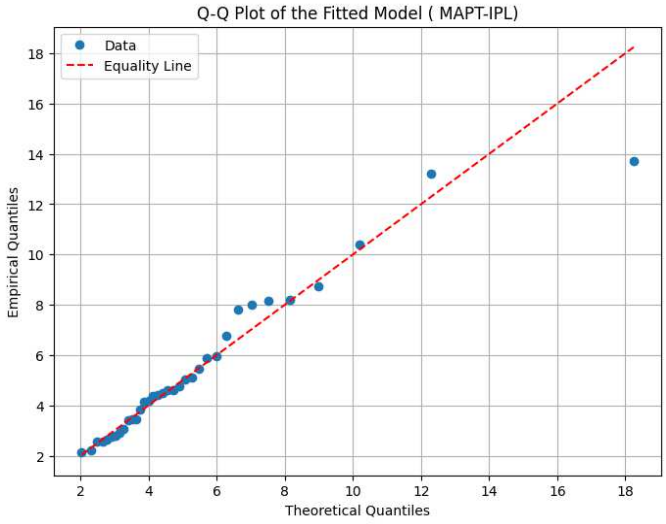

Q-Q plot

Fig. 12: Graphical representation of the hazard rate and Q-Q plot for MAPT-IPL (dataset II)

CAIC, BIC, HQIC, and the Kolmogorov-Smirnov (K-S) statistic—are reported in Tables 6, 10, and 13. Across all datasets, the MAPT-IPL model consistently achieves the lowest values for these criteria. This result reflects its ability to provide an optimal trade-off between model complexity and goodness-of-fit, confirming the robustness and efficiency of the MAPT-IPL distribution.

The negative log-likelihood $\hat{l}$, a key measure of model adequacy, also supports the dominance of the MAPT-IPL model. For all datasets analyzed, the MAPT-IPL distribution achieves the smallest $\hat{l}$ values, indicating its exceptional fit to the data and its capacity to minimize residual error.

Furthermore, an in-depth assessment of the Q-Q plots for the MAPT-IPL model (Figure (9) , (**??**) and (**??**)) offers additional validation of its reliability. These plots, which compare the theoretical quantiles of the MAPT-IPL distribution with the empirical quantiles from the datasets, reveal an almost perfect alignment along the diagonal line. This near-perfect alignment emphasizes the MAPT-IPL model's ability to accurately represent the data distribution.The MAPT-IPL distribution's superior performance is particularly relevant for real-world applications, such as modeling service time data and other phenomena where precision and parsimony are critical. Its ability to deliver accurate fits without overcomplicating the model structure demonstrates its practical utility across various domains, including queue

© 2025 NSP
Natural Sciences Publishing Cor.

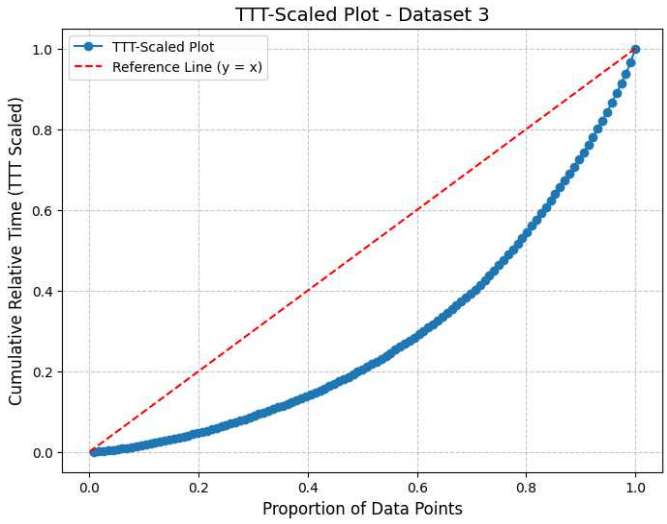

TTT-plot

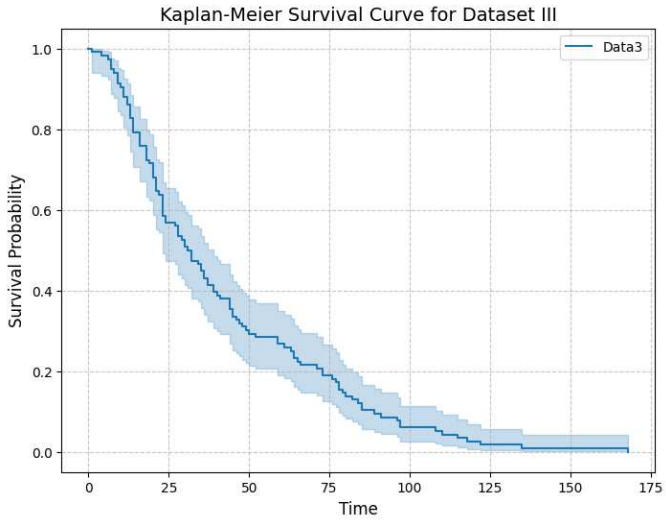

K-M plot

Fig. 13: Graphical representation of the TTT-scaled plot and Kaplan-Meier plot (Dataset III).

management, response time modeling, and other areas requiring effective probabilistic modeling. In summary, the MAPT-IPL distribution not only outperforms alternative models but also achieves this while maintaining a parsimonious design. This study underscores its relevance as a powerful tool for statistical modeling and encourages further exploration of its potential applications in diverse fields. The findings presented here reinforce the significant advantages of adopting the MAPT-IPL distribution in addressing complex real-world challenges.

9 Conclusion

In this study, we have introduced and investigated the MAPT-IPL distribution, a novel probability distribution tailored for modeling service time data in various practical scenarios. Through empirical analysis and comparison with existing models, including APTIL, APL, and IPL, we have demonstrated the superior performance of the MAPT-IPL distribution in terms of fit and parsimony.The results obtained from applying the MAPT-IPL distribution to real datasets underscore its effectiveness in capturing the underlying data structure accurately. This distribution outperformed its competitors across various evaluation criteria, including AIC, CAIC, BIC, HQIC, and negative log-likelihood, indicating its robustness and

© 2025 NSP
Natural Sciences Publishing Cor.

Table 13: Information criteria and additional statistics for the hailing time data (Dataset III)

Model	$-\hat{l}$	AIC	CAIC	BIC	HQIC	W	K-S	K-S (p-value)
MAPT-IPL	**538.64**	**1085.28**	**1097.29**	**1096.29**	**1089.75**	**0.8786**	**0.2398**	**0.0108**
MAPTW	540.87	1087.74	1099.00	1096.00	1091.09	0.8786	0.2146	0.0108
APTGE	541.09	1088.18	1099.44	1096.44	1091.53	0.8786	0.2149	0.0108
APTIL	542.18	1090.36	1101.62	1098.62	1093.72	0.8786	0.2106	0.0109
APTL	543.19	1092.38	1103.64	1100.64	1095.74	0.8786	0.2280	0.0108
IPL	544.24	1094.48	1105.74	1102.74	1097.84	0.8786	0.2301	0.0108

suitability for modeling service time phenomena.The advantages of the MAPT-IPL distribution lie in its ability to provide a balance between model complexity and goodness-of-fit, making it a valuable tool for practitioners and researchers alike. Its simplicity and flexibility make it applicable in a wide range of domains, including but not limited to queue management, computer systems modeling, telecommunications, and transportation.In conclusion, the MAPT-IPL distribution offers a promising approach for modeling service time data, with demonstrated advantages over existing models. Its potential for application in real-world scenarios makes it a valuable addition to the toolkit of statisticians, data scientists, and practitioners across various fields.

10 Future work

While the MAPT-IPL distribution shows promise in modeling service time data, there remain avenues for further exploration and refinement:

- –Investigation of specialized estimation techniques tailored to specific application domains, such as queue management, telecommunications, or transportation, to improve the accuracy and efficiency of parameter estimation for the MAPT-IPL distribution.
- –Extension of the MAPT-IPL distribution to accommodate additional parameters or features that may enhance its flexibility and descriptive power in capturing complex data patterns.
- –Application of the MAPT-IPL distribution to diverse datasets from various domains to assess its performance and robustness under different conditions and scenarios.
- –Exploration of advanced statistical inference methods and hypothesis testing procedures to derive insights and conclusions from data modeled using the MAPT-IPL distribution.
- –Developing user-friendly software packages or tools for estimating parameters, conducting inference, and performing goodness-of-fit tests using the MAPT-IPL distribution, thereby facilitating its adoption and use by practitioners and researchers in various fields.

By addressing these research directions, we can further refine and expand the applicability of the MAPT-IPL distribution, unlocking its full potential for modeling and analyzing service time phenomena across different practical contexts.

© 2025 NSP
Natural Sciences Publishing Cor.

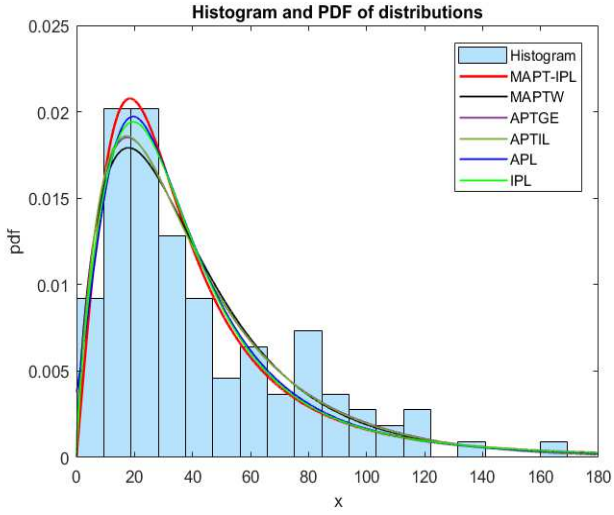

histogram and pdfs

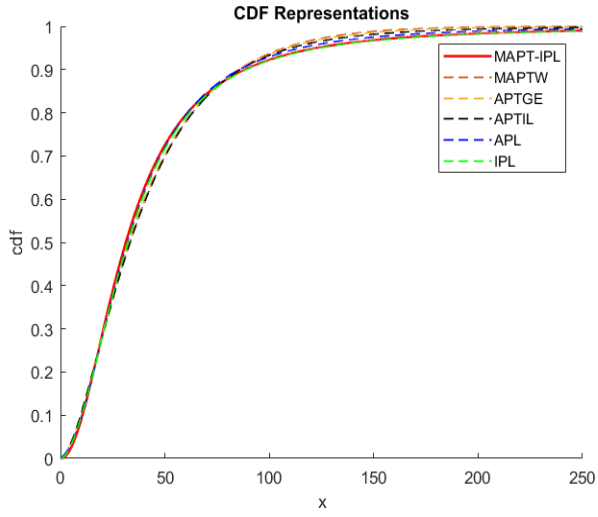

cdfs

Fig. 14: Graphical representation of the pdf and cdf (dataset III)

© 2025 NSP
Natural Sciences Publishing Cor.

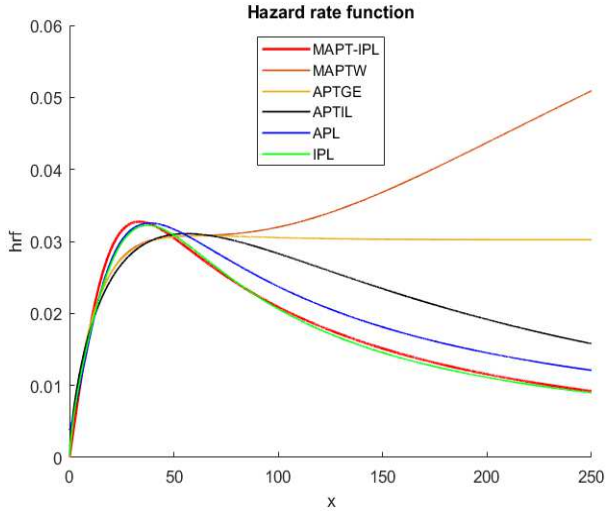

Illustration of hrf

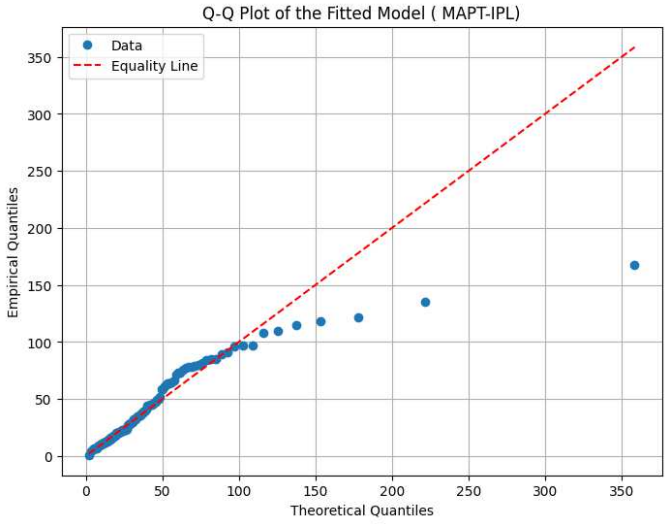

Q-Q plot

Fig. 15: Graphical representation of the hazard rate and Q-Q plot for MAPT-IPL (dataset III)

© 2025 NSP
Natural Sciences Publishing Cor.

References

[1] I. Elbatal, G. Ozel, S. Cakmakyapan, Odd extended exponential-g family: Properties and application on earthquake data, Journal of Statistics and Management Systems (2022) 1–15.

[2] R. O. Olanrewaju, On the application of generalized beta-g family of distributions to prices of cereals, Journal of Mathematical Finance 11 (4) (2021) 670–685.

[3] B. Hosseini, M. Afshari, M. Alizadeh, The generalized odd gamma-g family of distributions: properties and applications, Austrian Journal of Statistics 47 (2) (2018) 69–89.

[4] A. S. Hassan, E. M. Almetwally, G. M. Ibrahim, Kumaraswamy inverted topp–leone distribution with applications to covid-19 data, Computers, Materials, & Continua (2021) 337–358.

[5] H. Yousof, A. Z. Afify, M. Alizadeh, G. Hamedani, S. Jahanshahi, I. Ghosh, The generalized transmuted poisson-g family of distributions: Theory, characterizations and applications, Pakistan Journal of Statistics and Operation Research (2018) 759–779.

[6] R. A. Bantan, F. Jamal, C. Chesneau, M. Elgarhy, A new power topp–leone generated family of distributions with applications, Entropy 21 (12) (2019) 1177.

[7] M. N. Atchadé, M. J. Bogninou, A. M. Djibril, M. N'bouké, Topp-leone cauchy family of distributions with applications in industrial engineering, Journal of Statistical Theory and Applications 22 (4) (2023) 339–365.

[8] S. A. Alyami, I. Elbatal, N. Alotaibi, E. M. Almetwally, H. M. Okasha, M. Elgarhy, Topp–leone modified weibull model: Theory and applications to medical and engineering data, Applied Sciences 12 (20) (2022) 10431.

[9] P. E. Oguntunde, M. A. Khaleel, H. I. Okagbue, O. A. Odetunmibi, The topp–leone lomax (tllo) distribution with applications to airbone communication transceiver dataset, Wireless Personal Communications 109 (2019) 349–360.

[10] M. A. Khaleel, P. E. Oguntunde, J. N. Al Abbasi, N. A. Ibrahim, M. H. AbuJarad, The marshall-olkin topp leone-g family of distributions: A family for generalizing probability models, Scientific African 8 (2020) e00470.

[11] S. Nasiru, A. G. Abubakari, C. Chesneau, The arctan power distribution: Properties, quantile and modal regressions with applications to biomedical data, Mathematical and Computational Applications 28 (1) (2023) 25.

[12] A. S. Hassan, M. Elgarhy, Z. Ahmad, Type ii generalized topp-leone family of distributions: Properties and applications., Journal of data science 17 (4).

[13] H. Torabi, N. H. Montazeri, The logistic-uniform distribution and its applications, Communications in Statistics-Simulation and Computation 43 (10) (2014) 2551–2569.

[14] H. Torabi, N. M. Hedesh, The gamma-uniform distribution and its applications, kybernetika 48 (1) (2012) 16–30.

[15] V. Vatsal, Uniform distribution of heegner points, Inventiones mathematicae 148 (1) (2002) 1.

[16] E. Brito, G. Cordeiro, H. Yousof, M. Alizadeh, G. Silva, The topp–leone odd log-logistic family of distributions, Journal of Statistical Computation and Simulation 87 (15) (2017) 3040–3058.

[17] T. Moakofi, B. Oluyede, F. Chipepa, Type ii exponentiated half-logistic-topp-leone-g power series class of distributions with applications, Pakistan Journal of Statistics and Operation Research (2021) 885–909.

[18] S. Al-Marzouki, F. Jamal, C. Chesneau, M. Elgarhy, Type ii topp leone power lomax distribution with applications, Mathematics 8 (1) (2019) 4.

[19] F. Chipepa, B. Oluyede, D. Wanduku, T. Moakofi, The exponentiated half logistic-topp-leone-g power series class of distributions: Model, properties and applications, Methods of Mathematical Modelling and Computation for Complex Systems (2022) 341–374.

[20] N. Kunjiratanachot, W. Bodhisuwan, Extended generalized exponential power series distribution, in: AIP Conference Proceedings, Vol. 1905, AIP Publishing LLC, 2017, p. 050026.

[21] E. M. Almetwally, R. Alharbi, D. Alnagar, E. H. Hafez, A new inverted topp-leone distribution: applications to the covid-19 mortality rate in two different countries, Axioms 10 (1) (2021) 25.

[22] A. M. Gemeay, K. Karakaya, M. Bakr, O. S. Balogun, M. N. Atchadé, E. Hussam, Power lambert uniform distribution: Statistical properties, actuarial measures, regression analysis, and applications, AIP Advances 13 (9).

[23] A. Rahman, M. Kamal, S. Khan, M. F. Khan, M. S. Mustafa, E. Hussam, M. N. Atchadé, A. Al Mutairi, Statistical inferences under step stress partially accelerated life testing based on multiple censoring approaches using simulated and real-life engineering data, Scientific Reports 13 (1) (2023) 12452.

[24] M. N. Atchadé, M. N'bouké, A. M. Djibril, S. Shahzadi, E. Hussam, R. Aldallal, H. M. Alshanbari, A. M. Gemeay, A.-A. H. El-Bagoury, A new power topp–leone distribution with applications to engineering and industry data, PloS one 18 (1) (2023) e0278225.

[25] K. Sakthivel, K. Dhivakar, Type ii power topp-leone daggum distribution with application in reliability, Reliability: Theory & Applications 16 (2 (62)) (2021) 136–156.

[26] A. Ahmad, N. Alsadat, M. N. Atchade, S. Q. ul Ain, A. M. Gemeay, M. A. Meraou, E. M. Almetwally, M. M. Hossain, E. Hussam, New hyperbolic sine-generator with an example of rayleigh distribution: Simulation and data analysis in industry, Alexandria Engineering Journal 73 (2023) 415–426.

[27] A. A. Ogunde, O. E. Adeniji, Type ii topp-leone bur xii distribution: Properties and applications to failure time data, Scientific African 16 (2022) e01200.

© 2025 NSP
Natural Sciences Publishing Cor.

[28] A. Pourdarvish, S. Mirmostafaee, K. Naderi, The exponentiated topp-leone distribution: Properties and application, Journal of Applied Environmental and Biological Sciences 5 (7) (2015) 251–256.
[29] E.-S. A. El-Sherpieny, M. A. Ahmed, On the kumaraswamy kumaraswamy distribution, International Journal of Basic and Applied Sciences 3 (4) (2014) 372.
[30] M. S. Khan, R. King, I. L. Hudson, Transmuted kumaraswamy distribution, Statistics in Transition new series 2 (17) (2016) 183–210.
[31] A. J. Lemonte, W. Barreto-Souza, G. M. Cordeiro, The exponentiated kumaraswamy distribution and its log-transform.
[32] A. Abd AL-Fattah, A. El-Helbawy, G. Al-Dayian, Inverted kumaraswamy distribution: Properties and estimation., Pakistan Journal of Statistics 33 (1).
[33] J. Mazucheli, A. Menezes, L. Fernandes, R. De Oliveira, M. Ghitany, The unit-weibull distribution as an alternative to the kumaraswamy distribution for the modeling of quantiles conditional on covariates, Journal of Applied Statistics 47 (6) (2020) 954–974.
[34] F. Cribari-Neto, J. Santos, Inflated kumaraswamy distributions, Anais da Academia Brasileira de Ciências 91.
[35] Z. Iqbal, M. M. Tahir, N. Riaz, S. A. Ali, M. Ahmad, Generalized inverted kumaraswamy distribution: properties and application, Open Journal of Statistics 7 (4) (2017) 645–662.
[36] W. Barreto-Souza, A. J. Lemonte, Bivariate kumaraswamy distribution: properties and a new method to generate bivariate classes, Statistics 47 (6) (2013) 1321–1342.
[37] F. Chipepa, B. Oluyede, B. Makubate, et al., The topp-leone-marshall-olkin-g family of distributions with applications, International Journal of Statistics and Probability 9 (4) (2020) 15–32.
[38] M. Elgarhy, M. Arslan Nasir, F. Jamal, G. Ozel, The type ii topp-leone generated family of distributions: Properties and applications, Journal of Statistics and Management Systems 21 (8) (2018) 1529–1551.
[39] B. Oluyede, S. Chamunorwa, F. Chipepa, M. Alizadeh, The topp-leone gompertz-g family of distributions with applications, Journal of Statistics and Management Systems 25 (6) (2022) 1399–1423.
[40] D. Vicari, J. R. Van Dorp, S. Kotz, Two-sided generalized topp and leone (ts-gtl) distributions, Journal of Applied Statistics 35 (10) (2008) 1115–1129.
[41] R. M. Usman, M. A. ul Haq, The marshall-olkin extended inverted kumaraswamy distribution: Theory and applications, Journal of King Saud University-Science 32 (1) (2020) 356–365.
[42] R. George, S. Thobias, Marshall-olkin kumaraswamy distribution, in: International Mathematical Forum, Vol. 12, 2017, pp. 47–69.
[43] A. Akinsete, F. Famoye, C. Lee, The kumaraswamy-geometric distribution, Journal of statistical distributions and applications 1 (1) (2014) 1–21.
[44] T. V. F. De Santana, E. M. Ortega, G. M. Cordeiro, G. O. Silva, The kumaraswamy-log-logistic distribution, Journal of Statistical Theory and Applications 11 (3) (2012) 265–291.
[45] M. Bourguignon, R. Silva, L. Zea, G. Cordeiro, The kumaraswamy pareto distribution, J. Stat. Theory Appl 12 (2).
[46] H. Reyad, F. Jamal, S. Othman, N. Yahia, The topp leone generalized inverted kumaraswamy distribution: Properties and applications, Asian Research Journal of Mathematics 13 (3) (2019) 1–15.
[47] A. S. Hassan, M. Abd-Allah, On the inverse power lomax distribution, Annals of Data Science 6 (2019) 259–278.
[48] A. Mahdavi, D. Kundu, A new method for generating distributions with an application to exponential distribution, Communications in Statistics-Theory and Methods 46 (13) (2017) 6543–6557.
[49] M. Nassar, A. Alzaatreh, M. Mead, O. Abo-Kasem, Alpha power weibull distribution: Properties and applications, Communications in Statistics-Theory and Methods 46 (20) (2017) 10236–10252.
[50] A. S. Hassan, R. E. Mohamd, M. Elgarhy, A. Fayomi, Alpha power transformed extended exponential distribution: properties and applications, Journal of Nonlinear Sciences and Applications 12 (4) (2018) 62–67.
[51] S. Dey, M. Nassar, D. Kumar, Alpha power transformed inverse lindley distribution: A distribution with an upside-down bathtub-shaped hazard function, Journal of Computational and Applied Mathematics 348 (2019) 130–145.
[52] J. T. Eghwerido, L. C. Nzei, F. I. Agu, The alpha power gompertz distribution: characterization, properties, and applications, Sankhya A 83 (1) (2021) 449–475.
[53] R. A. ZeinEldin, M. Ahsan ul Haq, S. Hashmi, M. Elsehety, Alpha power transformed inverse lomax distribution with different methods of estimation and applications, Complexity 2020 (2020) 1–15.
[54] Y. M. Amer, Alpha-power transformed lomax distribution: Properties and application.
[55] R. Alotaibi, H. Okasha, H. Rezk, M. Nassar, A new weighted version of alpha power transformation method: Properties and applications to covid-19 and software reliability data, Physica Scripta 96 (12) (2021) 125221.
[56] R. Alotaibi, H. Okasha, M. Nassar, A. Elshahhat, A novel modified alpha power transformed weibull distribution and its engineering applications, Comput. Model. Eng. Sci 135 (2023) 2065–2089.
[57] J. F. Kenney, Mathematics of statistics, D. van Nostrand, 1939.
[58] J. Moors, A quantile alternative for kurtosis, Journal of the Royal Statistical Society: Series D (The Statistician) 37 (1) (1988) 25–32.
[59] S. Nadarajah, I. E. Okorie, On the moments of the alpha power transformed generalized exponential distribution, Ozone: Science & Engineering 40 (4) (2018) 330–335.
[60] E. T. Lee, J. Wang, Statistical methods for survival data analysis, Vol. 476, John Wiley & Sons, 2003.
[61] B. Makubate, K. Rannona, B. Oluyede, F. Chipepa, The topp leone-g power series class of distributions with applications.

© 2025 NSP
Natural Sciences Publishing Cor.